MINISTRY OF HEALTH OF THE REPUBLIC OF UZBEKISTAN

KHUDAYBERGENOV GULOMBOY URUNOVICH

MODERN APPROACHES TO THE STUDY OFCOVID-19 ASSOCIATED CAVERNOUS SINUS THROMBOSIS

(MONOGRAPH)

URGENCH – 2025

UDC 616.8-06.9:616.1451..-005.6-07-088

Khudaybergenov G.U. Modern Approaches to the Study of COVID-19 Associated cavernous sinus thrombosis Urgench, 2025

Reviewers:

Niyazmetov B.K. — Senior lecturer of the department of Otorhinolaryngology and Ophthalmology, Urgench State Medical Institute

Radjapov A.A. — Head of the Department of Clinical Sciences, Mamun University

The monograph presents data from national and international researchers on the theoretical foundations of COVID-19–associated cavernous sinus thrombosis, as well as the author's own research findings and original methodological approaches.

The monograph is intended for practical use by ophthalmologists, general practitioners, clinical residents, and medical students.

CONTENTS

INTRODUCTION

At present, a considerable body of scientific evidence has accumulated indicating that *"...the SARS-CoV-2 virus, the causative agent of COVID-19, is capable of inducing various forms of ocular involvement, including lesions of the retina and optic nerve."* The course of the pandemic has demonstrated that the most severe ophthalmic complication associated with coronavirus infection is COVID-19–associated cavernous sinus thrombosis (CST). Under normal circumstances, CST is an extremely rare condition; however, during the results of such studies are expected to contribute significantly to the development of optimal clinical guidelines and management algorithms, the implementation of which is an important component of modern healthcare practice.

In the Republic of Uzbekistan, comprehensive measures aimed at developing the healthcare sector and improving the quality of medical services—aligned with international standards—are currently being implemented. Despite the end of the acute pandemic phase, nationwide programs continue to address complications of coronavirus infection and necrotic process within the maxillofacial structures, especially in the orbit and paranasal sinuses—factors that contribute significantly to high mortality rates. Given the substantial number of clinical cases, the study of the pathomorphological features of orbital and ocular involvement, correlated with the clinical presentation of this pathology, represents a research area of high scientific and practical relevance.

Worldwide, research on ophthalmic complications of COVID-19 continues. A special focus is directed toward the investigation of various aspects of the clinical course, diagnostics, treatment and prevention of COVID-19–associated CST. Despite the end of the acute pandemic phase, nationwide programs continue to address complications of coronavirus infection. The strategic priorities include the development and application of optimal methods for the treatment and prevention of COVID-19 complications, using advanced imaging techniques in combination with histopathological tissue analysis. The results of such studies are expected to contribute significantly to the development of optimal clinical

guidelines and management algorithms, the implementation of which is an important component of modern healthcare practice.

In the Republic of Uzbekistan, comprehensive measures aimed at developing the healthcare sector and improving the quality of medical services—aligned with international standards—are currently being implemented. Despite the end of the acute pandemic phase, nationwide programs continue to address complications of coronavirus infection. The strategic priorities include the development and application of optimal methods for the treatment and prevention of COVID-19 complications, as well as *"...the improvement of approaches to the control of infectious diseases, particularly coronavirus infection, and the enhancement of institutional and organizational frameworks of the sanitary-epidemiological service under current complex conditions and in light of the acquired experience..."*.

The disability, and mortality associated with this severe complication.

CHAPTER I. CURRENT KNOWLEDGE ON OCULAR INVOLVEMENT IN CORONAVIRUS INFECTION

§1.1. Fundamental Concepts of Coronavirus Infection and COVID-19

Mutations of SARS-CoV-2 resulting in new variants were detected in multiple countries:– B.1.1.7 in the United Kingdom (early 2020),– B.1.526 in the United States (November 2020),– B.1.525 in the United Kingdom and Nigeria (December 2020),– B.1.351 in South Africa (late 2020),– B.1.617.2 (Delta) in India (December 2020), becoming globally dominant by August 2021 due to a 40–60% increase in transmissibility,– B.1.1.529 (Omicron) identified in Botswana and South Africa (November 2021), noted for exceptionally rapid spread Early in the outbreak, both isolated case reports and clinical studies documented ocular symptoms—most notably conjunctival hyperemia and irritation—confirming that conjunctivitis may represent one of the ophthalmic manifestations of SARS-CoV-2 infection. As the pandemic progressed, accumulating evidence also linked COVID-19 to uveitis, retinal vascular abnormalities, and a variety of neuro-ophthalmic disorders [17, 20, 22, 25, p. 2950].

During the 2003 outbreak of severe acute respiratory syndrome (SARS), SARS-CoV was detected in tear samples from infected patients in Singapore. Lack of ocular protection was identified as a major risk factor for transmission of When the first systematic review was published, the U.S. Centers for Disease Control and Prevention (CDC) reported 337,278 confirmed cases and 9,637 deaths. A little over a year later, by April 16, 2021, global mortality had exceeded 3 million. The progression underscored the severity of the pandemic: the first million deaths occurred within 8.5 months of the initial fatal case in China, the second million accumulated over the following 3.5 months, and the third within an additional 3 months [42, p. 2470; 43; 44, p. 403].

Given this context, researchers aimed to consolidate current data on ocular manifestations of COVID-19 to improve early recognition, refine diagnostic approaches, and reduce transmission. SARS-CoV-2 is a novel, positive-sense single-stranded RNA beta-coronavirus responsible for COVID-19, initially traced

to an outbreak in Wuhan, Hubei Province, China. Direct contact with mucous membranes—including the ocular surface—has been identified as a potential route of infection [27, p. 722; 28, p. 1372; 31; 32, p. 750; 33; 35, p. 853].

Coronaviruses are known to cause severe ocular disease in animals, such as anterior uveitis, retinitis, vasculitis, and optic neuritis in cats and rodents. By contrast, ocular manifestations in humans are typically mild and infrequent, although reports of eye involvement in COVID-19 patients continue to accumulate. Definitive descriptions of ocular complications in MERS and SARS remain limited, despite previous detection of SARS-CoV in ocular secretions. Other human coronaviruses, however, are well-recognized causes of viral conjunctivitis [40, p. 1176].

At the time of the initial publication (April 4, 2020), the World Health Organization (WHO) reported 1,272,953 confirmed COVID-19 cases and 69,428 deaths globally, with 79,332 new cases registered within the preceding 24 hours [41]. Another important alteration consisted of pronounced tissue edema, leading to atrophy and disintegration of structural elements, while focal areas demonstrated necrobiosis. Observations showed that the pigment cells of the pigmented epithelium underwent atrophy and displacement, with some exhibiting degeneration and necrobiosis. In the anterior margin of the connective-tissue layer of the pigmented epithelium, coronavirus-induced changes included signs of mucoid and fibrinoid swelling within stromal vessels.

In the middle mesodermal layer, which is rich in blood vessels, pronounced circulatory disturbances were identified—namely venous hyperemia and hemorrhage. In the posterior pigment–muscle layer, pigment cells were found to be destroyed and fragmented, while muscle cells were in a state of involuntary contraction.

In some cases, lymphoproliferative immunopathological inflammation developed within the pigmented epithelium. A dense lymphoid infiltrate appeared in the anterior connective-tissue layer of the pigmented epithelium around the interstitial tissues and vessels. Lymphoid infiltrates were found predominantly around blood vessels, and lymphocytic thrombi were observed in some veins.

Microscopic examination of the pigmented epithelium, which forms part of the uveal tract, revealed several abnormalities, the most notable of which were pronounced vascular dilation, vascular congestion, and extravasation of blood into surrounding tissues (see Fig. 4.9).

In the middle mesodermal layer, rich in vessels, significant circulatory disturbances such as venous hyperemia and hemorrhage were detected. In the posterior pigment–muscle layer, pigment cells were destroyed and fragmented, and muscle cells were in a state of involuntary contraction. In several cases, lymphoproliferative immunopathological inflammation was noted within the pigmented epithelium. A dense lymphoid infiltrate was identified in the anterior connective-tissue layer surrounding interstitial tissues and vessels. These infiltrates were predominantly perivascular, and lymphocytic thrombi were observed in several veins (Fig. 4.10). Lymphoid infiltrates mainly formed around the blood vessels, and lymphocytic thrombi developed in some veins.

When the first systematic review was published, the U.S. Centers for Disease Control and Prevention (CDC) reported 337,278 confirmed cases and 9,637 deaths. A little over a year later, by April 16, 2021, global mortality had exceeded 3 million. The progression underscored the severity of the pandemic: the first million deaths occurred within 8.5 months of the initial fatal case in China, the second million accumulated over the following 3.5 months, and the third within an additional 3 months [42, p. 2470; 43; 44, p. 403].

By December 23, 2021, the United States had recorded 51,574,787 confirmed cases and 809,300 deaths. Globally, more than 276 million cases and 5,374,744 deaths had been reported. United Kingdom (early 2020),– B.1.526 in the United States (November 2020),– B.1.525 in the United Kingdom and Nigeria (December 2020),– B.1.351 in South Africa (late 2020),– B.1.617.2 the United States had recorded 51,574,787 confirmed cases and 809,300 deaths. Globally, more than 276 million cases and 5,374,744 deaths had been reported. [45, p. 167; 47, p. 222].

Mutations of SARS-CoV-2 resulting in new variants were detected in multiple countries:– B.1.1.7 in the United Kingdom (early 2020),– B.1.526 in the

United States (November 2020),– B.1.525 in the United Kingdom and Nigeria (December 2020),– B.1.351 in South Africa (late 2020),– B.1.617.2 (Delta) in India (December 2020), becoming globally dominant by August 2021 due to a 40–60% increase in transmissibility,– B.1.1.529 (Omicron) identified in Botswana and South Africa (November 2021), noted for exceptionally rapid spread [47, p. 221; 49, p. 0736; 51, p. 1620; 52; 57; 58].

§1.2. Ophthalmic manifestations of coronavirus infection

Initial studies suggested that ocular manifestations of COVID-19 are generally rare.. A meta-analysis conducted by Nasiri et al. in 2021 reported a pooled prevalence of all ocular manifestations in 7,300 patients with COVID-19 of 11.03%, with conjunctivitis being the most common ocular condition (88.8%). In the same meta-analysis, the most frequently reported symptoms were dry eye or foreign body sensation (16%), eye redness (13.3%), tearing (12.8%), and itching (12.6%) [59, p. 1050; 60; 61; 62].

A case series reported ocular symptoms in 12 of 38 hospitalized patients with COVID-19 in Hubei Province, China, corresponding to 31.6%. Among these 12 patients, 3 had conjunctival hyperemia, 7 had chemosis, 7 epiphora, and 7 increased discharge. Notably, in one patient epiphora was the first presenting sign of COVID-19. Of those with It is possible that local microbiologic and immunologic conditions were altered by avascular changes induced by thrombosis in the setting of SARS-CoV-2 infection [104, p. 1002; 106; 113, p. 1166]. Another important alteration consisted of pronounced tissue edema, leading to atrophy and disintegration of structural elements, while focal areas demonstrated necrobiosis. Observations showed that the pigment cells of the pigmented epithelium underwent atrophy and displacement, with some exhibiting degeneration and necrobiosis. In the anterior margin of the connective-tissue layer of the pigmented epithelium, coronavirus-induced changes included signs of mucoid and fibrinoid swelling within stromal vessels.

In the middle mesodermal layer, which is rich in blood vessels, pronounced circulatory disturbances were identified—namely venous hyperemia and hemorrhage. In the posterior pigment–muscle layer, pigment cells were found to

be destroyed and fragmented, while muscle cells were in a state of involuntary contraction.

In some cases, lymphoproliferative immunopathological inflammation developed within the pigmented epithelium. A dense lymphoid infiltrate appeared in the anterior connective-tissue layer of the pigmented epithelium around the interstitial tissues and vessels. Lymphoid infiltrates were found predominantly around blood vessels, and lymphocytic thrombi were observed in some veins.

Microscopic examination of the pigmented epithelium, which forms part of the uveal tract, revealed several abnormalities, the most notable of which were pronounced vascular dilation, vascular congestion, and extravasation of blood into surrounding tissues (see Fig. 4.9).

In the middle mesodermal layer, rich in vessels, significant circulatory disturbances such as venous hyperemia and hemorrhage were detected. In the posterior pigment–muscle layer, pigment cells were destroyed and fragmented, and muscle cells were in a state of involuntary contraction. In several cases, lymphoproliferative immunopathological inflammation was noted within the pigmented epithelium. A dense lymphoid infiltrate was identified in the anterior connective-tissue layer surrounding interstitial tissues and vessels. These infiltrates were predominantly perivascular, and lymphocytic thrombi were observed in several veins (Fig. 4.10). Lymphoid infiltrates mainly formed around the blood vessels, and lymphocytic thrombi developed in some veins.

There are also increasing reports of concomitant invasive fungal rhino-orbital mucormycosis co-infection in patients with COVID-19. These opportunistic pathogens may thrive in the hypoxic respiratory environment created by SARS-CoV-2, as hypoxia may facilitate their replication and pathogenicity. Moreover, the use of steroids and immunosuppressive therapy in severe COVID-19 can further compromise immune defenses and promote such infections.

Patients with poorly controlled diabetes, particularly those with diabetic ketoacidosis (DKA), are also at elevated risk for opportunistic infections. Hyperglycemia and ketoacidosis create favorable conditions for the growth and

proliferation of bacteria and other microorganisms, increasing infection risk. In addition, patients with diabetes frequently exhibit impaired immune function, further predisposing them to infection [9, p. 52; 17].

Singh et al. published a systematic review of 101 cases of COVID-19–associated mucormycosis. Most patients were male (79%); 80% of these patients, and nearly 60% of cases involved rhino-orbital disease [22; 25, p. 2963].

Another report described a 33-year-old woman who presented with orbital compartment syndrome due to concurrent COVID-19 and fulminant mucormycosis infection.

MRI-confirmed orbital myositis has also been reported in two separate patients with COVID-19 without evidence of concomitant bacterial infection. The authors proposed that possible mechanisms included either direct viral invasion of the orbit or virus-induced autoimmunity.

Similar mechanisms were suggested by Diaz et al., who reported a case of acute dacryoadenitis in a 22-year-old man with positive antibodies to SARS-CoV-2 who developed partial ophthalmoplegia. Physicians at our university treated a patient with typical signs and symptoms of dacryoadenitis coinciding with a positive nasopharyngeal COVID-19 test. The patient responded to a slow taper of systemic steroids over six weeks. A recently presented case series from our group also highlighted biopsy-proven chronic dacryoadenitis in a 57-year-old man with COVID-19 whose symptoms began one month after his viral illness. Other cases in this series included idiopathic inflammation in an anophthalmic socket [27, p. 723; 28, p. 1373].

Lacrimal system. Epiphora has been described as an initial manifestation in patients with COVID-19, presumably secondary to conjunctival inflammation. Direct involvement of the nasolacrimal system or lacrimal sac has not yet been reported.

Manifestations in neonates. Recent data support frequent ocular manifestations of SARS-CoV-2 infection in neonates. In a study by Pérez-Chimal et al. in Mexico, 15 neonates with positive nasopharyngeal RT-PCR tests were identified. All of these neonates exhibited ocular findings, most commonly

periocular edema (100%), followed by chemosis and hemorrhagic conjunctivitis (73%) and ciliary injection (53%). Unique findings included corneal edema in 6 neonates (40%), rubeosis iridis with posterior synechiae in 1 neonate, and posterior segment manifestations, including retinopathy of prematurity in 3 (20%) neonates. Vitreous hemorrhage was observed in one term neonate, and subtle cotton-wool spots were noted in two others [31, p. 1215; 33; 49; 58, p. 1295].

At present, It is possible that local microbiologic and immunologic conditions were altered by avascular changes induced by thrombosis in the setting of SARS-CoV-2 infection [104, p. 1002; 106; 113, p. 1166].

There are also increasing reports of concomitant invasive fungal rhino-orbital mucormycosis co-infection in patients with COVID-19. These opportunistic pathogens may thrive in the hypoxic respiratory environment created by SARS-CoV-2, as hypoxia may facilitate their replication and pathogenicity. Moreover, the use of steroids and immunosuppressive therapy in severe COVID-19 can further compromise immune defenses and promote such infections.

Patients with poorly controlled diabetes, particularly those with diabetic ketoacidosis (DKA), are also at elevated risk for opportunistic infections. Hyperglycemia and ketoacidosis create favorable conditions for the growth and proliferation of bacteria and other microorganisms, increasing infection risk. In addition, patients with diabetes frequently exhibit impaired immune function, further predisposing them to infection [9, p. 52; 17].

Singh et al. published a systematic review of 101 cases of COVID-19–associated mucormycosis. Most patients were male (79%); 80% of these patients, and nearly 60% of cases involved rhino-orbital disease [22; 25, p. 2963].

Another report described a 33-year-old woman who presented with orbital compartment syndrome due to concurrent COVID-19 and fulminant mucormycosis infection.

MRI-confirmed orbital myositis has also been reported in two separate patients with COVID-19 without evidence of concomitant bacterial infection. The

authors proposed that possible mechanisms included either direct viral invasion of the orbit or virus-induced autoimmunity.

Similar mechanisms were suggested by Diaz et al., who reported a case of acute dacryoadenitis in a 22-year-old man with positive antibodies to SARS-CoV-2 who developed partial ophthalmoplegia. Physicians at our university treated a patient with typical signs and symptoms of dacryoadenitis coinciding with a positive nasopharyngeal COVID-19 test. The patient responded to a slow taper of systemic steroids over six weeks. A recently presented case series from our group also highlighted biopsy-proven chronic dacryoadenitis in a 57-year-old man with COVID-19 whose symptoms began one month after his viral illness. Other cases in this series included idiopathic inflammation in an anophthalmic socket [27, p. 723; 28, p. 1373].

Lacrimal system. Epiphora has been described as an initial manifestation in patients with COVID-19, presumably secondary to conjunctival inflammation. Direct involvement of the nasolacrimal system or lacrimal sac has not yet been reported.

Manifestations in neonates. Recent data support frequent ocular manifestations of SARS-CoV-2 infection in neonates. In a study by Pérez-Chimal et al. in Mexico, 15 neonates with positive nasopharyngeal RT-PCR tests were identified. All of these neonates exhibited ocular findings, most commonly periocular edema (100%), followed by chemosis and hemorrhagic conjunctivitis (73%) and ciliary injection (53%). Unique findings included corneal edema in 6 neonates (40%), rubeosis iridis with posterior synechiae in 1 neonate, and posterior segment manifestations, including retinopathy of prematurity in 3 (20%) neonates. Vitreous hemorrhage was observed in one term neonate, and subtle cotton-wool spots were noted in two others [31, p. 1215; 33; 49; 58, p. 1295].

In another observation, a 46-year-old man with mild respiratory symptoms developed bilateral hemorrhagic conjunctivitis 5 days after a positive COVID-19 test. The left eye had been enucleated several years earlier due to melanoma. Hemorrhagic conjunctivitis with chemosis and pseudomembrane formation on the conjunctiva of the ocular prosthesis was also noted. Treatment with topical

antibiotics led to resolution of symptoms within four weeks. No other symptoms of COVID-19 were observed in this patient [120, p. 1023; 121; 122].

It should also Retina and choroid. A possible association between posterior segment disease and COVID-19 infection has also been suggested. These conditions have varied etiologies, including vascular, inflammatory, and neuronal mechanisms. ACE2 and TMPRSS2 receptors, which are highly expressed in the human retina, have become a focus of investigation. A recent case series of three patients identified COVID-19 S and N proteins in retinal vascular endothelial cells by immunofluorescence microscopy, indicating the presence of viral particles. Cases of central retinal vein occlusion (CRVO) and central retinal artery occlusion (CRAO) have also been reported in patients without typical systemic vascular risk factors. The proposed mechanisms include complement-mediated inflammation and virus-induced inflammatory processes leading to endothelial damage and a microangiopathic state. A striking example was described by Walinjkar et al., who reported CRVO in a 17-year-old girl with COVID-19. Yahalomi et al. presented a similar case in a previously healthy 33-year-old patient. Several cases of CRAO have also been documented, potentially related to virus-induced endothelial injury and vasculitis [132; 133; 134; 135].

Furthermore, acute macular neuroretinopathy (AMN) and paracentral acute middle maculopathy (PAMM) have been identified in the setting of COVID-19. These conditions are characterized by ischemia of the deep retinal capillary plexus and appear as hyperreflective changes at the level of the outer plexiform and inner nuclear layers. In addition, two cases of retinopathy resembling Purtscher's retinopathy in patients with COVID-19 have been reported [136, p. 590].

Bottini et al. described a 59-year-old man who presented with multiple bilateral cotton-wool spots localized in the posterior pole after a month-long hospitalization for COVID-19 pneumonia complicated by multiorgan failure and severe coagulopathy. It is possible that local microbiologic and immunologic conditions were altered by avascular changes induced by thrombosis in the setting of SARS-CoV-2 infection [104, p. 1002; 106; 113, p. 1166].

There are also increasing reports of concomitant invasive fungal rhino-orbital mucormycosis co-infection in patients with COVID-19. These opportunistic pathogens may thrive in the hypoxic respiratory environment created by SARS-CoV-2, as hypoxia may facilitate their replication and pathogenicity. Moreover, the use of steroids and immunosuppressive therapy in severe COVID-19 can further compromise immune defenses and promote such infections.

Another important alteration consisted of pronounced tissue edema, leading to atrophy and disintegration of structural elements, while focal areas demonstrated necrobiosis. Observations showed that the pigment cells of the pigmented epithelium underwent atrophy and displacement, with some exhibiting degeneration and necrobiosis. In the anterior margin of the connective-tissue layer of the pigmented epithelium, coronavirus-induced changes included signs of mucoid and fibrinoid swelling within stromal vessels.

In the middle mesodermal layer, which is rich in blood vessels, pronounced circulatory disturbances were identified—namely venous hyperemia and hemorrhage. In the posterior pigment–muscle layer, pigment cells were found to be destroyed and fragmented, while muscle cells were in a state of involuntary contraction.

In some cases, lymphoproliferative immunopathological inflammation developed within the pigmented epithelium. A dense lymphoid infiltrate appeared in the anterior connective-tissue layer of the pigmented epithelium around the interstitial tissues and vessels. Lymphoid infiltrates were found predominantly around blood vessels, and lymphocytic thrombi were observed in some veins.

Microscopic examination of the pigmented epithelium, which forms part of the uveal tract, revealed several abnormalities, the most notable of which were pronounced vascular dilation, vascular congestion, and extravasation of blood into surrounding tissues (see Fig. 4.9).

In the middle mesodermal layer, rich in vessels, significant circulatory disturbances such as venous hyperemia and hemorrhage were detected. In the posterior pigment–muscle layer, pigment cells were destroyed and fragmented,

and muscle cells were in a state of involuntary contraction. In several cases, lymphoproliferative immunopathological inflammation was noted within the pigmented epithelium. A dense lymphoid infiltrate was identified in the anterior connective-tissue layer surrounding interstitial tissues and vessels. These infiltrates were predominantly perivascular, and lymphocytic thrombi were observed in several veins (Fig. 4.10). Lymphoid infiltrates mainly formed around the blood vessels, and lymphocytic thrombi developed in some veins.

Patients with poorly controlled diabetes, particularly those with diabetic ketoacidosis (DKA), are also at elevated risk for opportunistic infections. Hyperglycemia and ketoacidosis create favorable conditions for the growth and proliferation of bacteria and other microorganisms, increasing infection risk. In addition, patients with diabetes frequently exhibit impaired immune function, further predisposing them to infection [9, p. 52; 17].

Singh et al. published a systematic review of 101 cases of COVID-19–associated mucormycosis. Most patients were male (79%); 80% of these patients, and nearly 60% of cases involved rhino-orbital disease [22; 25, p. 2963].

Another report described a 33-year-old woman who presented with orbital compartment syndrome due to concurrent COVID-19 and fulminant mucormycosis infection.

MRI-confirmed orbital myositis has also been reported in two separate patients with COVID-19 without evidence of concomitant bacterial infection. The authors proposed that possible mechanisms included either direct viral invasion of the orbit or virus-induced autoimmunity.

Similar mechanisms were suggested by Diaz et al., who reported a case of acute dacryoadenitis in a 22-year-old man with positive antibodies to SARS-CoV-2 who developed partial ophthalmoplegia. Physicians at our university treated a patient with typical signs and symptoms of dacryoadenitis coinciding with a positive nasopharyngeal COVID-19 test. The patient responded to a slow taper of systemic steroids over six weeks. A recently presented case series from our group also highlighted biopsy-proven chronic dacryoadenitis in a 57-year-old man with COVID-19 whose symptoms began one month after his viral illness. Other cases

in this series included idiopathic inflammation in an anophthalmic socket [27, p. 723; 28, p. 1373]. Manifestations in neonates. Recent data support frequent ocular manifestations of SARS-CoV-2 infection in neonates. In a study by Pérez-Chimal et al. in Mexico, 15 neonates with positive nasopharyngeal RT-PCR tests were identified. All of these neonates exhibited ocular findings, most commonly periocular edema (100%), followed by chemosis and hemorrhagic conjunctivitis (73%) and ciliary injection (53%). Unique findings included corneal edema in 6 neonates (40%), rubeosis iridis with posterior synechiae in 1 neonate, and posterior segment manifestations, including retinopathy of prematurity in 3 (20%) neonates. Vitreous hemorrhage was observed in one term neonate, and subtle cotton-wool spots were noted in two others [31, p. 1215; 33; 49; 58, p. 1295].

Lacrimal system. Epiphorapresumably secondary to conjunctival inflammation. Direct involvement of the nasolacrimal system or lacrimal sac has not yet been reported.

Manifestations in neonates. Recent data support frequent ocular manifestations of SARS-CoV-2 infection in neonates. In a study by Pérez-Chimal et al. in Mexico, 15 neonates with positive nasopharyngeal RT-PCR tests were identified. All of these neonates exhibited ocular findings, most commonly periocular edema (100%), followed by chemosis and hemorrhagic conjunctivitis (73%) and ciliary injection (53%). Unique findings included corneal edema in 6 neonates (40%), rubeosis iridis with posterior synechiae in 1 neonate, and posterior segment manifestations, including retinopathy of prematurity in 3 (20%) neonates. Vitreous hemorrhage was observed in one term neonate, and subtle cotton-wool spots were noted in two others [31, p. 1215; 33; 49; 58, p. 1295].and positive cultures for *Streptococcus constellatus* and *Peptoniphilus indolicus*—bacteria that are typically absent from the orbit and upper respiratory mucosa. It is possible that local microbiologic and immunologic conditions were altered by avascular changes induced by thrombosis in the setting of SARS-CoV-2 infection [104, p. 1002; 106; 113, p. 1166].

There are also increasing reports of concomitant invasive fungal rhino-orbital mucormycosis co-infection in patients with COVID-19. These opportunistic pathogens may thrive in the hypoxic respiratory environment created by SARS-CoV-2, as hypoxia may facilitate their replication and pathogenicity. Moreover, the use of steroids and immunosuppressive therapy in severe COVID-19 can further compromise immune defenses and promote such infections.

Patients with poorly controlled diabetes, particularly those with diabetic ketoacidosis (DKA), are also at elevated risk for opportunistic infections. Hyperglycemia and ketoacidosis create favorable conditions for the growth and proliferation of bacteria and other microorganisms, increasing infection risk. In addition, patients with diabetes frequently exhibit impaired immune function, further predisposing them to infection [9, p. 52; 17].

Singh et al. published a systematic review of 101 cases of COVID-19–associated mucormycosis. Most patients were male (79%); 80% of these patients, and nearly 60% of cases involved rhino-orbital disease [22; 25, p. 2963].

Another report described a 33-year-old woman who presented with orbital compartment syndrome due to concurrent COVID-19 and fulminant mucormycosis infection.

MRI-confirmed orbital myositis has also been reported in two separate patients with COVID-19 without evidence of concomitant bacterial infection. The authors proposed that possible mechanisms included either direct viral invasion of the orbit or virus-induced autoimmunity.

Similar mechanisms were suggested by Diaz et al., who reported a case of acute dacryoadenitis in a 22-year-old man with positive antibodies to SARS-CoV-2 who developed partial ophthalmoplegia. Physicians at our university treated a patient with typical signs and symptoms of dacryoadenitis coinciding with a positive nasopharyngeal COVID-19 test. The patient responded to a slow taper of systemic steroids over six weeks. A recently presented case series from our group also highlighted biopsy-proven chronic dacryoadenitis in a 57-year-old man with COVID-19 whose symptoms began one month after his viral illness. Other cases

in this series included idiopathic inflammation in an anophthalmic socket [27, p. 723; 28, p. 1373].

Lacrimal system. Epiphorapresumably secondary to conjunctival inflammation. Direct involvement of the nasolacrimal system or lacrimal sac has not yet been reported.

Manifestations in neonates. Recent data support frequent ocular manifestations of SARS-CoV-2 infection in neonates. In a study by Pérez-Chimal et al. in Mexico, 15 neonates with positive nasopharyngeal RT-PCR tests were identified. All of these neonates exhibited ocular findings, most commonly periocular edema (100%), followed by chemosis and hemorrhagic conjunctivitis (73%) and ciliary injection (53%). Unique findings included corneal edema in 6 neonates (40%), rubeosis iridis with posterior synechiae in 1 neonate, and posterior segment manifestations, including retinopathy of prematurity in 3 (20%) neonates. Vitreous hemorrhage was observed in one term neonate, and subtle cotton-wool spots were noted in two others [31, p. 1215; 33; 49; 58, p. 1295].

§1.3. Fundamentals of the etiopathogenesis, clinical features, and pathomorphology of cavernous sinus thrombosis

By December 23, 2021, the United States had recorded 51,574,787 confirmed cases and 809,300 deaths. Globally, more than 276 million cases and 5,374,744 deaths had been reported. United Kingdom (early 2020),– B.1.526 in the United States (November 2020),– B.1.525 in the United Kingdom and Nigeria (December 2020),– B.1.351 in South Africa (late 2020),– B.1.617.2 the United States had recorded 51,574,787 confirmed cases and 809,300 deaths. Globally, more than 276 million cases and 5,374,744 deaths had been reported. [45, p. 167; 47, p. 222].

Mutations of SARS-CoV-2 resulting in new variants were detected in multiple countries:– B.1.1.7 in the United Kingdom (early 2020),– B.1.526 in the United States (November 2020),– B.1.525 in the United Kingdom and Nigeria (December 2020),– B.1.351 in South Africa (late 2020),– B.1.617.2 (Delta) in India (December 2020), becoming globally dominant by August 2021 due to a 40–60% increase in transmissibility,– B.1.1.529 (Omicron) identified in

Botswana and South Africa (November 2021), noted for exceptionally rapid spread [47, p. 221; 49, p. 0736; 51, p. 1620; 52; 57; 58]. Another important alteration consisted of pronounced tissue edema, leading to atrophy and disintegration of structural elements, while focal areas demonstrated necrobiosis. Observations showed that the pigment cells of the pigmented epithelium underwent atrophy and displacement, with some exhibiting degeneration and necrobiosis. In the anterior margin of the connective-tissue layer of the pigmented epithelium, coronavirus-induced changes included signs of mucoid and fibrinoid swelling within stromal vessels.

In the middle mesodermal layer, which is rich in blood vessels, pronounced circulatory disturbances were identified—namely venous hyperemia and hemorrhage. In the posterior pigment–muscle layer, pigment cells were found to be destroyed and fragmented, while muscle cells were in a state of involuntary contraction.

In some cases, lymphoproliferative immunopathological inflammation developed within the pigmented epithelium. A dense lymphoid infiltrate appeared in the anterior connective-tissue layer of the pigmented epithelium around the interstitial tissues and vessels. Lymphoid infiltrates were found predominantly around blood vessels, and lymphocytic thrombi were observed in some veins.

Microscopic examination of the pigmented epithelium, which forms part of the uveal tract, revealed several abnormalities, the most notable of which were pronounced vascular dilation, vascular congestion, and extravasation of blood into surrounding tissues (see Fig. 4.9).

In the middle mesodermal layer, rich in vessels, significant circulatory disturbances such as venous hyperemia and hemorrhage were detected. In the posterior pigment–muscle layer, pigment cells were destroyed and fragmented, and muscle cells were in a state of involuntary contraction. In several cases, lymphoproliferative immunopathological inflammation was noted within the pigmented epithelium. A dense lymphoid infiltrate was identified in the anterior connective-tissue layer surrounding interstitial tissues and vessels. These infiltrates were predominantly perivascular, and lymphocytic thrombi were

observed in several veins (Fig. 4.10). Lymphoid infiltrates mainly formed around the blood vessels, and lymphocytic thrombi developed in some veins.

Examination of the ciliary body revealed the development of marked circulatory, inflammatory, and destructive–necrotic alterations, which were most frequently identified on histological sections (see Fig. 4.11). The circulatory disturbances were characterized by dilation of blood vessels, tissue edema, and atrophy, accompanied by hemorrhages in certain areas. As a result, compression, deformation, and structural alterations were identified, leading to dystrophic and necrotic changes in some of the muscular lamellae of the ciliary body. The muscle fibers of the ciliary body were dilated and deformed; signs of mucoid and fibrinoid swelling, as well as necrosis, were detected within its stroma. Detachment of the ciliary body's basal membrane from the sclera and its deformation were also observed, caused by edema associated with fibrinoid swelling and fibrinoid necrosis.

In some cases, the mesodermal portion of the ciliary body exhibited predominant lymphoid infiltration and vascular atrophy (Fig. 4.12). As a result, signs of dystrophy and destruction of pigment cells within the ciliary body were identified.

In the course of studying the pathomorphological changes occurring in the ocular tissues as a result of SARS-CoV-2–related complications, special attention—following the vascular layer—was directed to the retina. It was established that in most cases, the retina became detached from the underlying choroid, accompanied by extensive hemorrhage. Within the surrounding blood, lymphoid cells were identified in addition to plasma cells and erythrocytes. The retina was found to be deformed and focally condensed in certain areas (Fig. 4.13).

It should be noted that in various cases of retinal involvement, severe hemorrhages were also detected within the choroid, along with profound tissue and cellular alterations leading to destruction and necrosis (Fig. 4.14). The choroid and the nuclear layers of the retina were also edematous, with destruction of cellular and tissue structures, resulting in a disruption of normal histotopography. Similar changes were observed in the outer plexiform and nuclear layers. The subsequent

inner nuclear layer and internal limiting membrane showed deformed cell nuclei clustered into large accumulations. The ganglion cell layer was extensively damaged, with partial loss of neuronal cells, while the intercellular spaces became edematous and vacuolated. The outer limiting membrane was not identifiable, and the inner retinal layers were intermixed with blood, lacking any organized structural pattern (Fig. 4.15). During microscopic examination of the optic nerve, attention must be paid to its histotopographic architecture and structural composition. The nerve fibers are surrounded by a thick outer sheath—the epineurium—and each nerve fiber is encased by the perineurium, which consists of specialized membranes containing sensory neuronal elements.

Microscopic evaluation of optic nerve fibers damaged as a result of venous sinus thrombosis of the brain in the context of COVID-19 revealed that the external epineurial sheath, composed of connective tissue and associated cells, was edematous and had lost its normal histotopography. Both within and outside this sheath, inflammatory infiltrates were present. Within the epineurium, areas of pronounced dilation of nerve fibers were observed (Fig. 4.16).

Each nerve fiber bundle within the perineurium, formed by specialized cells, demonstrated a reduction in volume due to dystrophic changes in the perineurial cells. Cytoplasmic edema was identified in each fiber bundle, indicating vacuolization. The nerve fibers were structurally damaged and deformed.The sclera is a dense, tightly arranged, non-transparent outer coat of the eyeball. Externally, it is connected to the venous vessels via the episclera. The middle layer consists of fibrocytes and collagen fibers characteristic of the sclera. Within the coat lies a thin layer of blood vessels containing pigmented chromophore cells, which impart coloration to the structure.

United Kingdom (early 2020),– B.1.526 in the United States (November 2020),– B.1.525 in the United Kingdom and Nigeria (December 2020),– B.1.351 in South Africa (late 2020),– B.1.617.2 (Delta) in India (December 2020), becoming globally dominant by August 2021 due to a 40–60% increase in transmissibility,– B.1.1.529 (Omicron) identified in Botswana and South Africa (November 2021), noted for exceptionally rapid spread Early in the outbreak, both

isolated case reports and clinical studies documented ocular symptoms—most notably conjunctival hyperemia and irritation—confirming that conjunctivitis may represent one of the ophthalmic manifestations of SARS-CoV-2 infection. As the pandemic progressed, accumulating evidence also linked COVID-19 to uveitis, retinal vascular abnormalities, and a variety of neuro-ophthalmic disorders [17, 20, 22, 25, p. 2950].

During the 2003 outbreak of severe acute respiratory syndrome (SARS), SARS-CoV was detected in tear samples from infected patients in Singapore. Lack of ocular protection was identified as a major risk factor for transmission of When the first systematic review was published, the U.S. Centers for Disease Control and Prevention (CDC) reported 337,278 confirmed cases and 9,637 deaths. A little over a year later, by April 16, 2021, global mortality had exceeded 3 million. The progression underscored the severity of the pandemic: the first million deaths occurred within 8.5 months of the initial fatal case in China, the second million accumulated over the following 3.5 months, and the third within an additional 3 months [42, p. 2470; 43; 44, p. 403].

Given this context, researchers aimed to consolidate current data on ocular manifestations of COVID-19 to improve early recognition, refine diagnostic approaches, and reduce transmission. SARS-CoV-2 is a novel, positive-sense single-stranded RNA beta-coronavirus responsible for COVID-19, initially traced to an outbreak in Wuhan, Hubei Province, China. Direct contact with mucous membranes—including the ocular surface—has been identified as a potential route of infection [27, p. 722; 28, p. 1372; 31; 32, p. 750; 33; 35, p. 853].

Coronaviruses are known to cause severe ocular disease in animals, such as anterior uveitis, retinitis, vasculitis, and optic neuritis in cats and rodents. By contrast, ocular manifestations in humans are typically mild and infrequent, although reports of eye involvement in COVID-19 patients continue to accumulate. Definitive descriptions of ocular complications in MERS and SARS remain limited, despite previous detection of SARS-CoV in ocular secretions. Other human coronaviruses, however, are well-recognized causes of viral conjunctivitis [40, p. 1176].

At the time of the initial publication (April 4, 2020), the World Health Organization (WHO) reported 1,272,953 confirmed COVID-19 cases and 69,428 deaths globally, with 79,332 new cases registered within the preceding 24 hours [41].

When the first systematic review was published, the U.S. Centers for Disease Control and Prevention (CDC) reported 337,278 confirmed cases and 9,637 deaths. A little over a year later, by April 16, 2021, global mortality had exceeded 3 million. The progression underscored the severity of the pandemic: the first million deaths occurred within 8.5 months of the initial fatal case in China, the second million accumulated over the following 3.5 months, and the third within an additional 3 months [42, p. 2470; 43; 44, p. 403].

By December 23, 2021, the United States had recorded 51,574,787 confirmed cases and 809,300 deaths. Globally, more than 276 million cases and 5,374,744 deaths had been reported. United Kingdom (early 2020),– B.1.526 in the United States (November 2020),– B.1.525 in the United Kingdom and Nigeria (December 2020),– B.1.351 in South Africa (late 2020),– B.1.617.2 the United States had recorded 51,574,787 confirmed cases and 809,300 deaths. Globally, more than 276 million cases and 5,374,744 deaths had been reported. [45, p. 167; 47, p. 222].

Mutations of SARS-CoV-2 resulting in new variants were detected in multiple countries:– B.1.1.7 in the United Kingdom (early 2020),– B.1.526 in the United States (November 2020),– B.1.525 in the United Kingdom and Nigeria (December 2020),– B.1.351 in South Africa (late 2020),– B.1.617.2 (Delta) in India (December 2020), becoming globally dominant by August 2021 due to a 40–60% increase in transmissibility,– B.1.1.529 (Omicron) identified in Botswana and South Africa (November 2021), noted for exceptionally rapid spread [47, p. 221; 49, p. 0736; 51, p. 1620; 52; 57; 58]. Another important alteration consisted of pronounced tissue edema, leading to atrophy and disintegration of structural elements, while focal areas demonstrated necrobiosis. Observations showed that the pigment cells of the pigmented epithelium underwent atrophy and displacement, with some exhibiting degeneration and

necrobiosis. In the anterior margin of the connective-tissue layer of the pigmented epithelium, coronavirus-induced changes included signs of mucoid and fibrinoid swelling within stromal vessels.

In the middle mesodermal layer, which is rich in blood vessels, pronounced circulatory disturbances were identified—namely venous hyperemia and hemorrhage. In the posterior pigment–muscle layer, pigment cells were found to be destroyed and fragmented, while muscle cells were in a state of involuntary contraction.

In some cases, lymphoproliferative immunopathological inflammation developed within the pigmented epithelium. A dense lymphoid infiltrate appeared in the anterior connective-tissue layer of the pigmented epithelium around the interstitial tissues and vessels. Lymphoid infiltrates were found predominantly around blood vessels, and lymphocytic thrombi were observed in some veins.

Microscopic examination of the pigmented epithelium, which forms part of the uveal tract, revealed several abnormalities, the most notable of which were pronounced vascular dilation, vascular congestion, and extravasation of blood into surrounding tissues (see Fig. 4.9).

In the middle mesodermal layer, rich in vessels, significant circulatory disturbances such as venous hyperemia and hemorrhage were detected. In the posterior pigment–muscle layer, pigment cells were destroyed and fragmented, and muscle cells were in a state of involuntary contraction. In several cases, lymphoproliferative immunopathological inflammation was noted within the pigmented epithelium. A dense lymphoid infiltrate was identified in the anterior connective-tissue layer surrounding interstitial tissues and vessels. These infiltrates were predominantly perivascular, and lymphocytic thrombi were observed in several veins (Fig. 4.10). Lymphoid infiltrates mainly formed around the blood vessels, and lymphocytic thrombi developed in some veins.

Examination of the ciliary body revealed the development of marked circulatory, inflammatory, and destructive–necrotic alterations, which were most frequently identified on histological sections (see Fig. 4.11). The circulatory disturbances were characterized by dilation of blood vessels, tissue edema, and atrophy,

accompanied by hemorrhages in certain areas. As a result, compression, deformation, and structural alterations were identified, leading to dystrophic and necrotic changes in some of the muscular lamellae of the ciliary body. The muscle fibers of the ciliary body were dilated and deformed; signs of mucoid and fibrinoid swelling, as well as necrosis, were detected within its stroma. Detachment of the ciliary body's basal membrane from the sclera and its deformation were also observed, caused by edema associated with fibrinoid swelling and fibrinoid necrosis.

In some cases, the mesodermal portion of the ciliary body exhibited predominant lymphoid infiltration and vascular atrophy (Fig. 4.12). As a result, signs of dystrophy and destruction of pigment cells within the ciliary body were identified. In the course of studying the pathomorphological changes occurring in the ocular tissues as a result of SARS-CoV-2–related complications, special attention—following the vascular layer—was directed to the retina. It was established that in most cases, the retina became detached from the underlying choroid, accompanied by extensive hemorrhage. Within the surrounding blood, lymphoid cells were identified in addition to plasma cells and erythrocytes. The retina was found to be deformed and focally condensed in certain areas (Fig. 4.13).

It should be noted that in various cases of retinal involvement, severe hemorrhages were also detected within the choroid, along with profound tissue and cellular alterations leading to destruction and necrosis (Fig. 4.14). The choroid and the nuclear layers of the retina were also edematous, with destruction of cellular and tissue structures, resulting in a disruption of normal histotopography. Similar changes were observed in the outer plexiform and nuclear layers. The subsequent inner nuclear layer and internal limiting membrane showed deformed cell nuclei clustered into large accumulations. The ganglion cell layer was extensively damaged, with partial loss of neuronal cells, while the intercellular spaces became edematous and vacuolated. The outer limiting membrane was not identifiable, and the inner retinal layers were intermixed with blood, lacking any organized structural pattern (Fig. 4.15). During microscopic examination of the optic nerve,

attention must be paid to its histotopographic architecture and structural composition. The nerve fibers are surrounded by a thick outer sheath—the epineurium—and each nerve fiber is encased by the perineurium, which consists of specialized membranes containing sensory neuronal elements.

Microscopic evaluation of optic nerve fibers damaged as a result of venous sinus thrombosis of the brain in the context of COVID-19 revealed that the external epineurial sheath, composed of connective tissue and associated cells, was edematous and had lost its normal histotopography. Both within and outside this sheath, inflammatory infiltrates were present. Within the epineurium, areas of pronounced dilation of nerve fibers were observed (Fig. 4.16).

Each nerve fiber bundle within the perineurium, formed by specialized cells, demonstrated a reduction in volume due to dystrophic changes in the perineurial cells. Cytoplasmic edema was identified in each fiber bundle, indicating vacuolization. The nerve fibers were structurally damaged and deformed.The sclera is a dense, tightly arranged, non-transparent outer coat of the eyeball. Externally, it is connected to the venous vessels via the episclera. The middle layer consists of fibrocytes and collagen fibers characteristic of the sclera. Within the coat lies a thin layer of blood vessels containing pigmented chromophore cells, which impart coloration to the structure.

CHAPTER II. MATERIALS AND METHODS

The study was conducted within the framework of the state applied research project“Development of comprehensive measures for the diagnosis, treatment, prognosis and prevention of COVID-19–associated cavernous sinus thrombosis” (A-CC-202110145).

Clinical material was collected from November 2020 to August 2022 at the Departments of Ophthalmology, Otorhinolaryngology, and Maxillofacial Surgery of the Multidisciplinary Clinic of the Tashkent Medical Academy (TMA).

§2.1. Characteristics of the clinical material

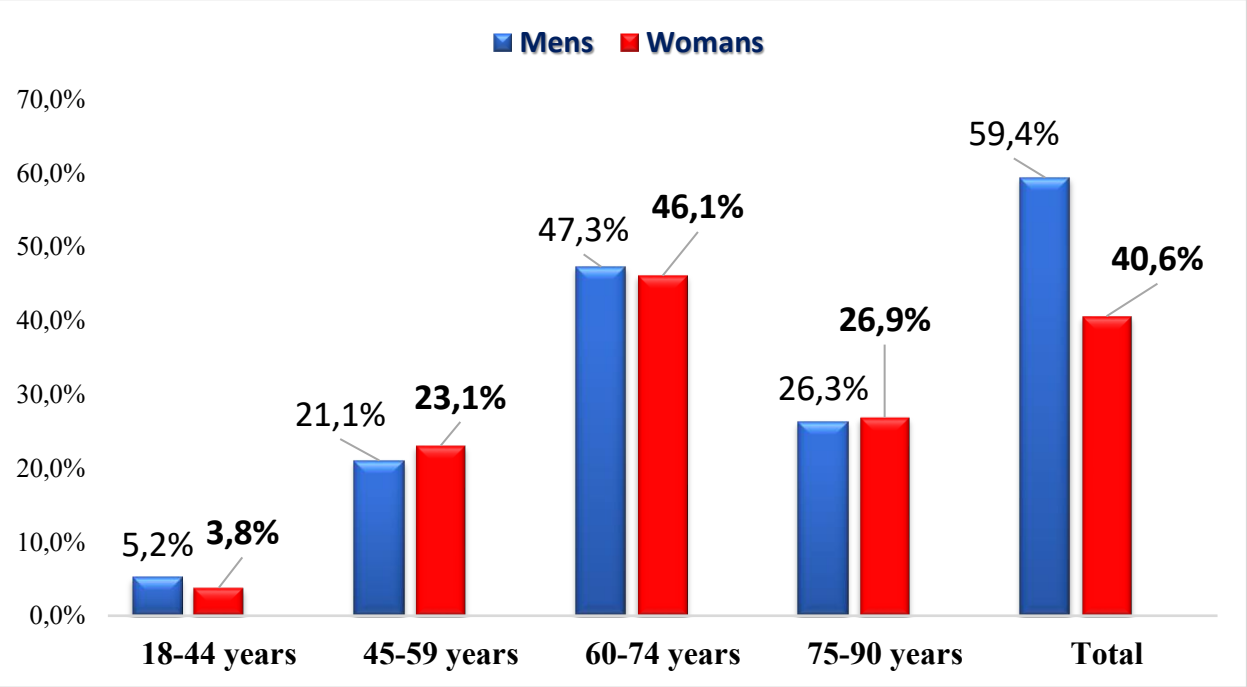

Figure 2.1. Distribution of patients by sex and age, %.

§ 2.2. Organization of the Study

The study design is presented in Figure 2.1.

The research consisted of three stages:

1. Stage I – Evaluation of the clinical characteristics of symptoms associated with involvement of the orbital structures and the eyeball.
2. Stage II – Assessment of signs of orbital and ocular involvement using specialized medical imaging techniques.
3. Stage III – Pathomorphological examination of material obtained after surgical intervention, including fragments of orbital bone structures, soft tissues of the orbit, and the eyeball.

4. Due to its complex neurovascular anatomy, cavernous sinus thrombosis (CST) represents the most severe form of intracranial venous thrombosis. The cavernous sinus is a paired anatomical structure located at the skull base along the lateral surfaces of the sella turcica.
5. Typically, the diagnosis is confirmed based on characteristic ophthalmic manifestations such as ptosis, exophthalmos, ophthalmoplegia, and loss of eyelid skin sensitivity. However, confirming the diagnosis only after these symptoms become clinically evident may be excessively late for initiating effective therapy. This delay is critical because the presence of such symptoms reflects damage to the oculomotor nerves, which, in cases of COVID-19–associated CST, is often irreversible.
6. Given that conventional imaging modalities do not always allow reliable visualization of the thrombus and that contrast enhancement may lead to uneven distribution of contrast medium with potential misinterpretation of the findings, a more detailed radiological protocol was proposed by Bilalov E.N., Oripov O.I., Umarov R.Z. (2020).
This approach includes assessment not only of the cavernous sinus, but also of the orbital veins and the orbital cavity. The technique utilizes specialized T2 TSE and Dark Fluid T2 MRI sequences with thin slices ranging from 0.6 to 1.6 mm.
7. High-resolution three-dimensional thin-slice acquisitions in T2 mode allow visualization of individual cranial nerves within the cavernous sinus and adjacent basal cisterns. TSE and Dark Fluid T2 sequences are routinely used for imaging the orbits and optic nerves. Standard scanning parameters typically include:
TR: 9000 ms, TE: 105 ms, TI: 2500 ms, FOV: 230 mm, Matrix: 210 × 256, Flip angle: 180°, Slice thickness: 3 mm, Number of slices: 12, Scan time: 4 min 39 s.

Figure 2.2. Study Design

§ 2.3. Research Methods

All patients underwent a comprehensive set of clinical, laboratory, and instrumental examinations.

The standard examination protocol for each patient included the following components:

- Ophthalmologic examination;
- Otorhinolaryngological assessment, including endoscopic examination of the nasal cavity and paranasal sinuses (PNS);
- Maxillofacial surgical evaluation — assessment of the condition of the teeth, hard palate, and maxilla, both visually and using CT data;
- Neurological or neurosurgical consultation, including evaluation of the fifth (V) and seventh (VII) cranial nerves (CN) and assessment of encephalitic symptoms;
- Instrumental investigations, which comprised:
    - MRI of the cerebral sinuses;
    - MRI of the orbit and optic nerve;
    - Multislice computed tomography (MSCT) of the cerebral sinuses;
    - MSCT of the maxillofacial region.
- Laboratory investigations, including:
    - Complete blood count (CBC);
    - Urinalysis;
    - Biochemical blood analysis (ferritin, C-reactive protein (CRP), procalcitonin, ALT, AST, glucose);
    - Coagulation profile;
    - D-dimer testing.
- Consultations with specialists — endocrinologist, hematologist, or intensivist — were conducted as clinically indicated.

2.3.1. Ophthalmologic Examination Methods

The study enrolled patients with varying degrees of systemic severity, and examinations were performed across different medical institutions and departments. Consequently, the list of standard ophthalmological procedures varied depending on the technical feasibility at each site.

Standard ophthalmic assessment included:

History taking and evaluation of complaints.

During anamnesis collection, specific attention was paid to:

- patient age;
- the relationship of symptoms to coronavirus infection—development of symptoms during a confirmed COVID-19 illness or during hospitalization in a COVID-19 treatment center;
- laterality of the process (unilateral or bilateral);
- timing of symptom onset;
- potential triggers or precipitating factors.

External examination.

During inspection of the orbital region, the following parameters were assessed:

- presence of ptosis;
- signs of periorbital cellulitis;
- lagophthalmos;
- exophthalmos;
- chemosis.

To determine the degree of ptosis, the following classification was applied:

- Partial ptosis — the upper eyelid margin is positioned at the upper third of the pupil;
- Incomplete ptosis — the eyelid margin reaches the mid-pupillary level;
- Complete ptosis — the upper eyelid fully covers the pupil.

Assessment of cutaneous sensitivity in the paraorbital region.

This test was performed to evaluate the function of the ophthalmic branch (V1) of the trigeminal nerve (cranial nerve V). Sensitivity was assessed by standard comparative testing on symmetrical facial areas. Additionally, sensitivity

of the zygomatic region and the presence of intraoral numbness—symptoms frequently detected—were evaluated.

Assessment of extraocular motility.

Eye movements were examined using standard protocols to detect partial or complete ophthalmoplegia. Facial muscle function was evaluated concurrently to identify possible involvement of cranial nerve VII.

Visual acuity testing (Visometry).

In patients with stable systemic conditions, visual acuity was measured in the ophthalmology office using the Golovin–Sivtsev charts, both without correction and with optimal refractive correction.
In patients with severe systemic status, the examination was performed at the bedside using Polyak optotypes.

Tonometry.

In the absence of chemosis or periorbital cellulitis, intraocular pressure was measured using the Maklakov method.

Exophthalmometry.

Proptosis measurement was performed using the Hertel exophthalmometer (Russia) (see Figure 2.1). The degree of globe protrusion was recorded in millimeters.

To grade the severity of exophthalmos, the 1976 classification by V. G. Baranov was applied:

- Grade I — exophthalmos from 15.0 ± 0.2 mm;
- Grade II — exophthalmos from 17.9 ± 0.2 mm;
- Grade III — marked exophthalmos up to 22.8 ± 1.1 mm.

Assessment of corneal sensitivity.

Performed using the standard technique by gently touching the cornea with a fine cotton wisp or a single delicate fiber while manually holding the eyelids open. The corneal response was graded using a “++++” scale to determine sensitivity level.

Evaluation of pupillary light response and detection of mydriasis.

This was performed using a “Heine” (Germany) electric ophthalmoscope.

Direct ophthalmoscopy.

Conducted with a direct electric ophthalmoscope (Heine, Germany).

Biomicroscopy of the anterior segment.

In patients with severe systemic conditions, anterior segment biomicroscopy was performed at the bedside using the handheld OP-2 electric ophthalmoscope (Russia) equipped with biomicroscopic and diaphanoscopic adapters.

In patients with stable physical status, the evaluation was performed in the ophthalmology office using a slit lamp (FSL 211, Carl Zeiss, Germany).

Figure 2.3. A. Huvitz HOCT-1F/1 optical coherence tomograph. B. Fundus color imaging mode (FUNDUS). C. Retinal cross-sectional scanning mode (OCT).

Optical coherence tomography was performed using the HOCT-1F/1 system manufactured by Huvitz (Republic of Korea) (see Figure 2.3). The examination protocol included:

- High-resolution color fundus photography in FUNDUS mode, and
- Cross-sectional retinal imaging (OCT mode) focused on the macular region and the optic nerve head.

2.3.2. Radiological Assessment Methods

Due to its complex neurovascular anatomy, cavernous sinus thrombosis (CST) represents the most severe form of intracranial venous thrombosis. The cavernous sinus is a paired anatomical structure located at the skull base along the lateral surfaces of the sella turcica.

Typically, the diagnosis is confirmed based on characteristic ophthalmic manifestations such as ptosis, exophthalmos, ophthalmoplegia, and loss of eyelid skin sensitivity. However, confirming the diagnosis only after these symptoms become clinically evident may be excessively late for initiating effective therapy. This delay is critical because the presence of such symptoms reflects damage to the oculomotor nerves, which, in cases of COVID-19–associated CST, is often irreversible.

Given that conventional imaging modalities do not always allow reliable visualization of the thrombus and that contrast enhancement may lead to uneven distribution of contrast medium with potential misinterpretation of the findings, a more detailed radiological protocol was proposed by Bilalov E.N., Oripov O.I., Umarov R.Z. (2020).
This approach includes assessment not only of the cavernous sinus, but also of the orbital veins and the orbital cavity. The technique utilizes specialized T2 TSE and Dark Fluid T2 MRI sequences with thin slices ranging from 0.6 to 1.6 mm.

High-resolution three-dimensional thin-slice acquisitions in T2 mode allow visualization of individual cranial nerves within the cavernous sinus and adjacent basal cisterns. TSE and Dark Fluid T2 sequences are routinely used for imaging the orbits and optic nerves. Standard scanning parameters typically include: TR: 9000 ms, TE: 105 ms, TI: 2500 ms, FOV: 230 mm, Matrix: 210 × 256, Flip angle: 180°, Slice thickness: 3 mm, Number of slices: 12, Scan time: 4 min 39 s.

The essence of the proposed technique lies in significantly reducing slice thickness to enhance spatial resolution for detecting intraorbital pathology. Imaging in this mode allows clear visualization of:

- thrombus formation within the orbital veins,
- orbital soft-tissue infiltrates,

- optic nerve edema.

Advantages of this MRI protocol

- Early detection of cavernous sinus thrombosis before overt clinical manifestation.
- No requirement for contrast agents, making the method more economical and safer.
- Thin-slice acquisition enables identification of venous congestion or thrombus in the projection of the affected orbital vein.
- Unlike MSCT, MRI avoids radiation exposure.

A International Patent Certificate for Utility Model (EU-01-003382) was granted for this visualization method (see Fig. 2.5).

MRI evaluation for this study was performed using a Siemens 1.5-T high-field scanner at the “AkfaMedLine” clinic.

Pathomorphological examination

Surgical specimens were collected intraoperatively. Due to its complex neurovascular anatomy, cavernous sinus thrombosis (CST) represents the most severe form of intracranial venous thrombosis. The cavernous sinus is a paired anatomical structure located at the skull base along the lateral surfaces of the sella turcica.

Typically, the diagnosis is confirmed based on characteristic ophthalmic manifestations such as ptosis, exophthalmos, ophthalmoplegia, and loss of eyelid skin sensitivity. However, confirming the diagnosis only after these symptoms become clinically evident may be excessively late for initiating effective therapy. This delay is critical because the presence of such symptoms reflects damage to the oculomotor nerves, which, in cases of COVID-19–associated CST, is often irreversible.

Given that conventional imaging modalities do not always allow reliable visualization of the thrombus and that contrast enhancement may lead to uneven distribution of contrast medium with potential misinterpretation of the findings, a more detailed radiological protocol was proposed by Bilalov E.N., Oripov O.I., Umarov R.Z. (2020).

This approach includes assessment not only of the cavernous sinus, but also of the orbital veins and the orbital cavity. The technique utilizes specialized T2 TSE and Dark Fluid T2 MRI sequences with thin slices ranging from 0.6 to 1.6 mm.

High-resolution three-dimensional thin-slice acquisitions in T2 mode allow visualization of individual cranial nerves within the cavernous sinus and adjacent basal cisterns. TSE and Dark Fluid T2 sequences are routinely used for imaging the orbits and optic nerves. Standard scanning parameters typically include: TR: 9000 ms, TE: 105 ms, TI: 2500 ms, FOV: 230 mm, Matrix: 210 × 256, Flip angle: 180°, Slice thickness: 3 mm, Number of slices: 12, Scan time: 4 min 39 s.

§ 2.4. Statistical Analysis of the Obtained Data

Statistical processing of the study results was performed using Microsoft Excel 2019. Methods of medical variational statistics were applied, including calculation of descriptive indicators such as the arithmetic mean of each parameter, standard deviation for relative values (frequency, %), and the standard error of the mean.

The statistical significance of differences between mean values was assessed using Student's t-test with estimation of the probability of error. Differences were considered statistically significant at a confidence level of $\mathbf{p < 0.05}$.

Data evaluation was conducted according to statistical approaches appropriate for **small sample sizes**.

CHAPTER III. CLINICAL PROFILE OF OCULAR AND ORBITAL INVOLVEMENT IN COVID-19–ASSOCIATED CAVERNOUS SINUS THROMBOSIS

Due to its complex neurovascular anatomy, cavernous sinus thrombosis (CST) represents the most severe form of intracranial venous thrombosis. The cavernous sinus is a paired anatomical structure located at the skull base along the lateral surfaces of the sella turcica.

Typically, the diagnosis is confirmed based on characteristic ophthalmic manifestations such as ptosis, exophthalmos, ophthalmoplegia, and loss of eyelid skin sensitivity. However, confirming the diagnosis only after these symptoms become clinically evident may be excessively late for initiating effective therapy. This delay is critical because the presence of such symptoms reflects damage to the oculomotor nerves, which, in cases of COVID-19–associated CST, is often irreversible.

Given that conventional imaging modalities do not always allow reliable visualization of the thrombus and that contrast enhancement may lead to uneven distribution of contrast medium with potential misinterpretation of the findings, a more detailed radiological protocol was proposed by Bilalov E.N., Oripov O.I., Umarov R.Z. (2020).
This approach includes assessment not only of the cavernous sinus, but also of the orbital veins and the orbital cavity. The technique utilizes specialized T2 TSE and Dark Fluid T2 MRI sequences with thin slices ranging from 0.6 to 1.6 mm.

High-resolution three-dimensional thin-slice acquisitions in T2 mode allow visualization of individual cranial nerves within the cavernous sinus and adjacent basal cisterns. TSE and Dark Fluid T2 sequences are routinely used for imaging the orbits and optic nerves. Standard scanning parameters typically include: TR: 9000 ms, TE: 105 ms, TI: 2500 ms, FOV: 230 mm, Matrix: 210 × 256, Flip angle: 180°, Slice thickness: 3 mm, Number of slices: 12, Scan time: 4 min 39 s.

visual loss, or proptosis. In addition, otorhinolaryngologists, maxillofacial surgeons, neurologists or neurosurgeons, hematologists, and intensivists may be required in the care of these patients. Given that many affected individuals present with severe systemic illness, the role of the intensivist is particularly important. Thus, COVID-19–related CST represents a complex clinical challenge encompassing multiple diagnostic and therapeutic dimensions. The ophthalmologist’s role is not limited to diagnosing and documenting ocular signs; in many cases, the ophthalmologist must also participate in decision-making regarding conservative management strategies.

Considering the above, the following sections also address the major risk factors and clinical manifestations of COVID-19–associated CST beyond the orbital structures.

§ 3.1. Clinical Characteristics of COVID-19–Associated CST in Patients

The scientific literature contains relatively few studies devoted specifically to cavernous sinus thrombosis. Existing publications describe a range of clinical forms of CST, which may vary depending on the anatomical location of the affected segment of the sinus.

Figure 3.1. Anatomical Structure of the Cavernous Sinus

The pattern of cranial nerve involvement varies according to the anatomical location of the lesion along the wall of the cavernous sinus: The scientific literature contains relatively few studies devoted specifically to cavernous sinus thrombosis. Existing publications describe a range of clinical forms of CST, which may vary depending on the anatomical location of the affected segment of the sinus.

Anterior Cavernous Sinus Syndrome

Involvement of the

Posterior Cavernous Sinus Syndrome

When the posterior segments of the cavernous sinus are affected, the lesion typically involves:

- cranial nerve VI, and
- all three divisions of the trigeminal nerve (V1, V2, V3).

The resulting clinical picture includes:

- diplopia,
- convergent paralytic strabismus,
- eyelid and conjunctival edema,
- prominent proptosis.

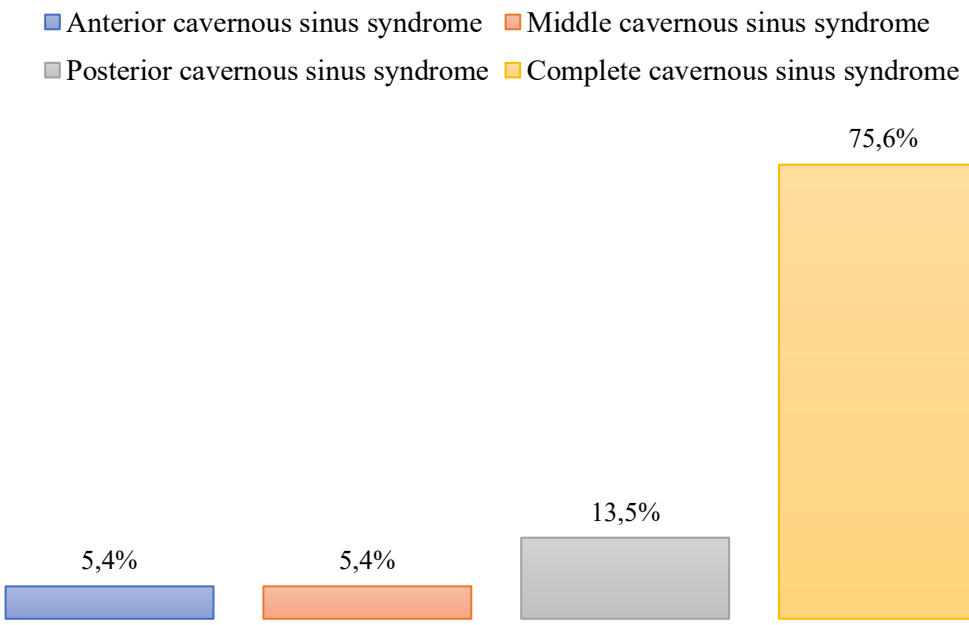

“Figure 3.2. Prevalence of clinical forms of COVID-19–associated cavernous sinus thrombosis.”

Analysis of the prevalence of various clinical forms of COVID-19–associated cavernous sinus thrombosis (CST) demonstrated that in most cases (75.6%), a complete cavernous sinus syndrome was observed, characterized by involvement of all oculomotor nerves as well as the first and second branches of the trigeminal nerve. The anterior cavernous sinus syndrome was identified in 5.4% of cases, the middle cavernous sinus syndrome in 5.4% of cases, and the posterior cavernous sinus syndrome in 13.5% of cases (Fig. 3.2). In syndromic variants of CST, the pathological process typically proceeds with a milder clinical course, in most cases with preservation of visual function and involvement of various cranial nerves depending on their topographic location.

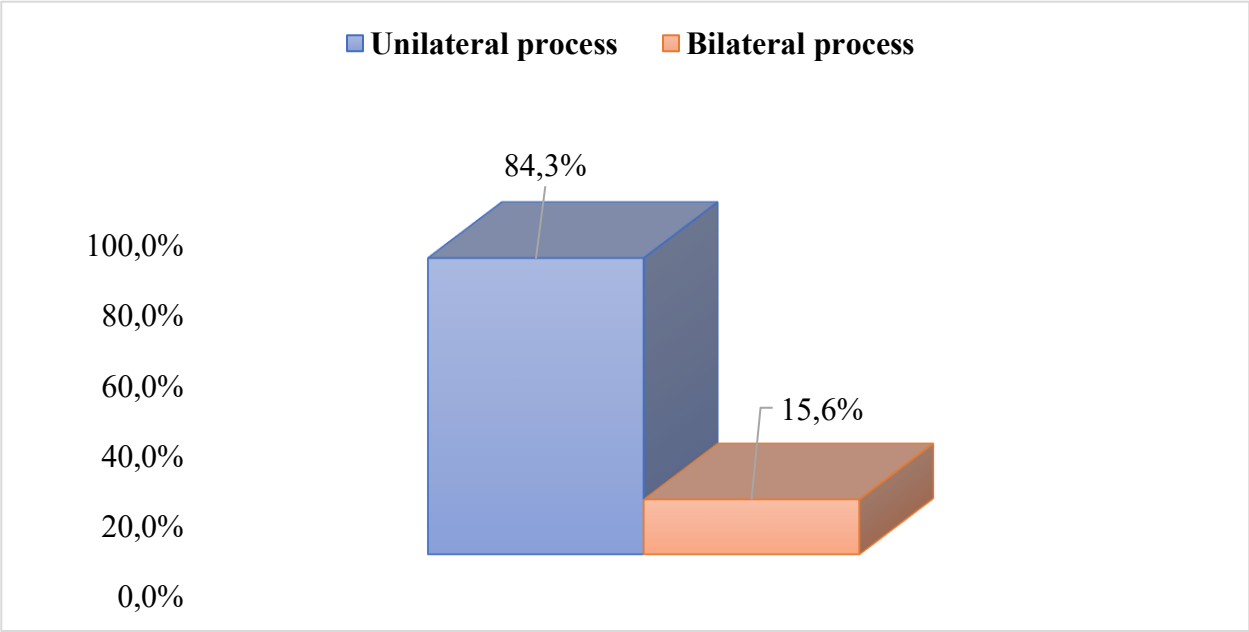

Figure 3.3. Frequency of pathological process extension to the contralateral eye.

Analysis of clinical cases of cavernous sinus thrombosis (CST) demonstrated that in 84.3% of cases, the pathological process was unilateral, whereas in 15.6% of cases, the process extended to the opposite eye, resulting in bilateral CST (Fig. 3.3). An investigation of the prevalence of superior orbital fissure symptoms showed that in 74 eyes affected by CST, classical components of the syndrome were observed in more than 70% of cases, including reduced sensitivity of the paraorbital skin, mydriasis, complete ophthalmoplegia, exophthalmos, and ptosis. Partial ophthalmoplegia was detected in 24% of eyes with syndromic variants of

CST (Fig. 3.4).

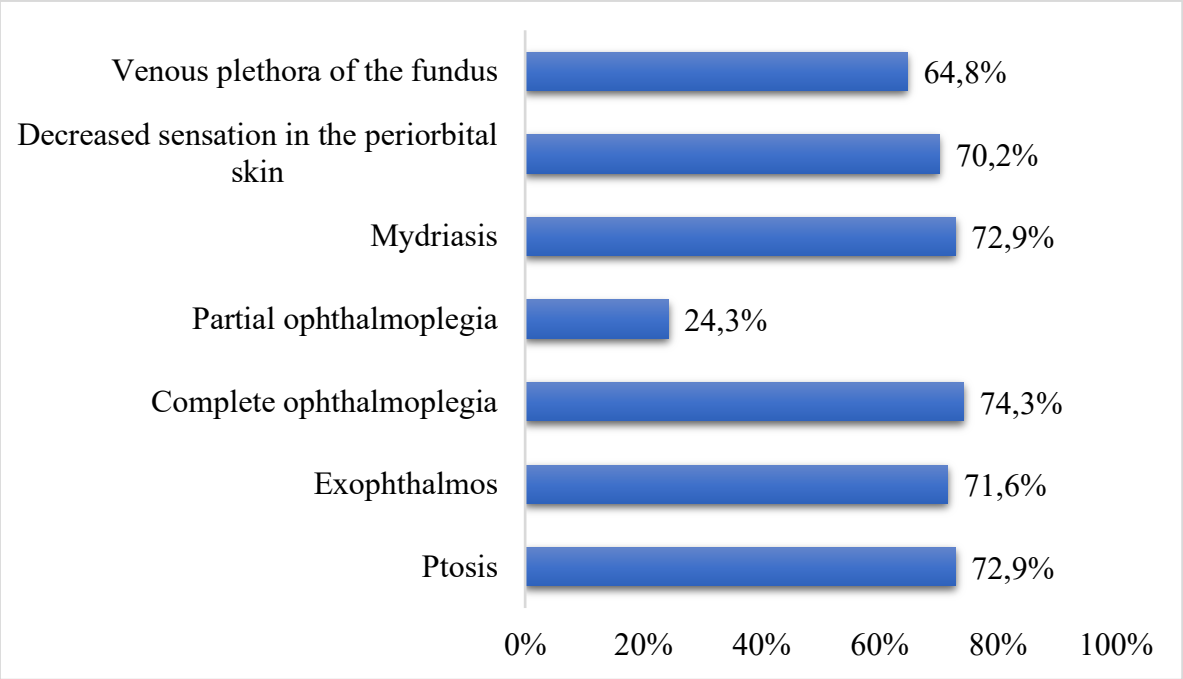

Figure 3.4. Frequency of symptoms of the superior orbital fissure (n = 74 eyes).

As is well known, two variants of clinical presentation can be distinguished in cavernous sinus thrombosis (CST), each following certain characteristic patterns: an aseptic (ischemic) variant, characterized by a slow progression of symptoms, and a septic variant, in which symptoms appear abruptly and rapidly worsen. Analysis of classical archival cases showed that the septic variant was observed in 70% of cases, whereas the aseptic variant was present in 30%, and these two forms could be clearly differentiated based on their clinical manifestations.

However, analysis of symptoms and their progression in cases of COVID-19–associated CST demonstrated that the clinical presentation of this condition cannot be unequivocally assigned to either variant.

In the majority of patients in the main group, a purulent-inflammatory process developed in the paranasal sinuses, progressing to a necrotic stage. Nevertheless, identifying which pathological process was primary proved difficult due to the simultaneous development of multiple symptoms.

Special attention should be given to the intensity of symptoms of periorbital cellulitis, reduced corneal sensitivity, and retinal edema. Analysis of archival data suggests that most patients exhibited classic clinical manifestations of CST.

Thus, the analyzed CST cases demonstrate a distinctive clinical course. They cannot be definitively classified as either aseptic or septic, as both a gradual progression of symptoms—characteristic of the aseptic variant—and signs of orbital phlegmon—suggestive of septic cavernous sinus thrombosis—were observed. However, it remains difficult to determine which process was primary: the development of purulent hemisinusitis with subsequent spread to the orbit, or cavernous sinus thrombosis followed by the development of a purulent-necrotic process in the paranasal sinuses.

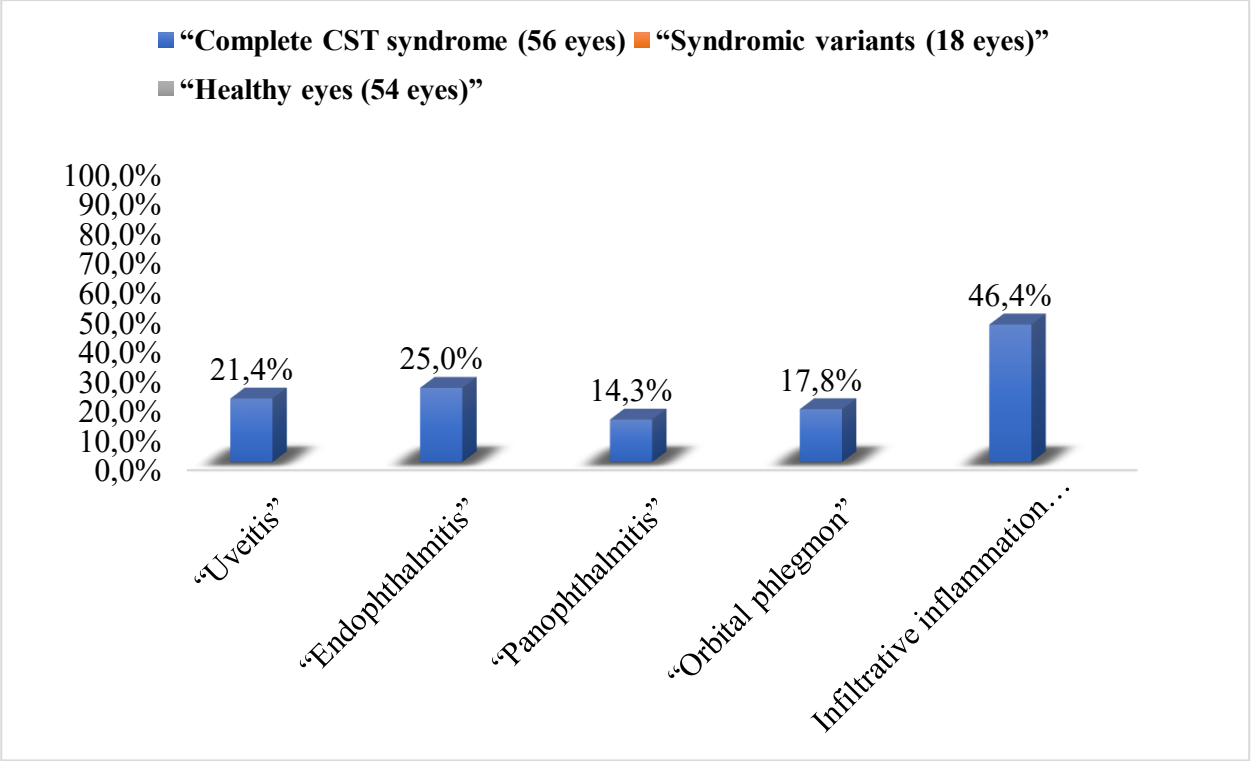

Figure 3.5. Structure of inflammatory process forms in the orbital structures and the eyeball.

Subsequently, randomization of eyes in the overall sample (128 eyes) was performed according to the type of pathological process into three groups: complete CST syndrome, syndromic CST variants, and the group of healthy eyes.

Analysis of the frequency of inflammatory process forms in the orbit and the eyeball showed that in 46% of eyes with complete CST, infiltrative inflammation of the orbital contents was observed, confirmed by MRI findings.

Orbital phlegmon developed in 17.8% of eyes. Inflammatory ocular pathologies such as uveitis, endophthalmitis, and panophthalmitis occurred considerably less frequently. It should be noted that none of these inflammatory forms were detected in eyes with syndromic variants of CST (Fig. 3.5).

§ 3.2. Clinical characteristics of eyeball involvement in patients with COVID-19–associated CST

Figure 3.6 illustrates the prevalence of individual clinical symptoms of inflammatory lesions of the eyeball and its adnexa. Particular attention should be paid to the relatively frequent development of inflammatory changes of the eyelids, conjunctiva, and paraorbital fat.

The clinical presentation of complete CST syndrome was characterized by predominance of conjunctival or mixed vascular injection. In 50% of eyes, conjunctivitis manifested with purulent discharge. Corneal precipitates were documented in more than 32.1% of eyes. Corneal erosion was noted in 10.7% of eyes. Hypopyon was present in 8.9%, and hyphema in 7.1%. Vitreous inflammation (vitritis) was observed in 25% of patients, which impeded ophthalmoscopy. Periorbital cellulitis was also recorded in 19.6% of eyes.

In eyes with syndromic variants of CST, conjunctival injection was observed in 75% of cases, pericorneal injection in 6.3%, purulent discharge in 12.5%, corneal precipitates in 6.3%, and vitritis in 12.5% of cases.

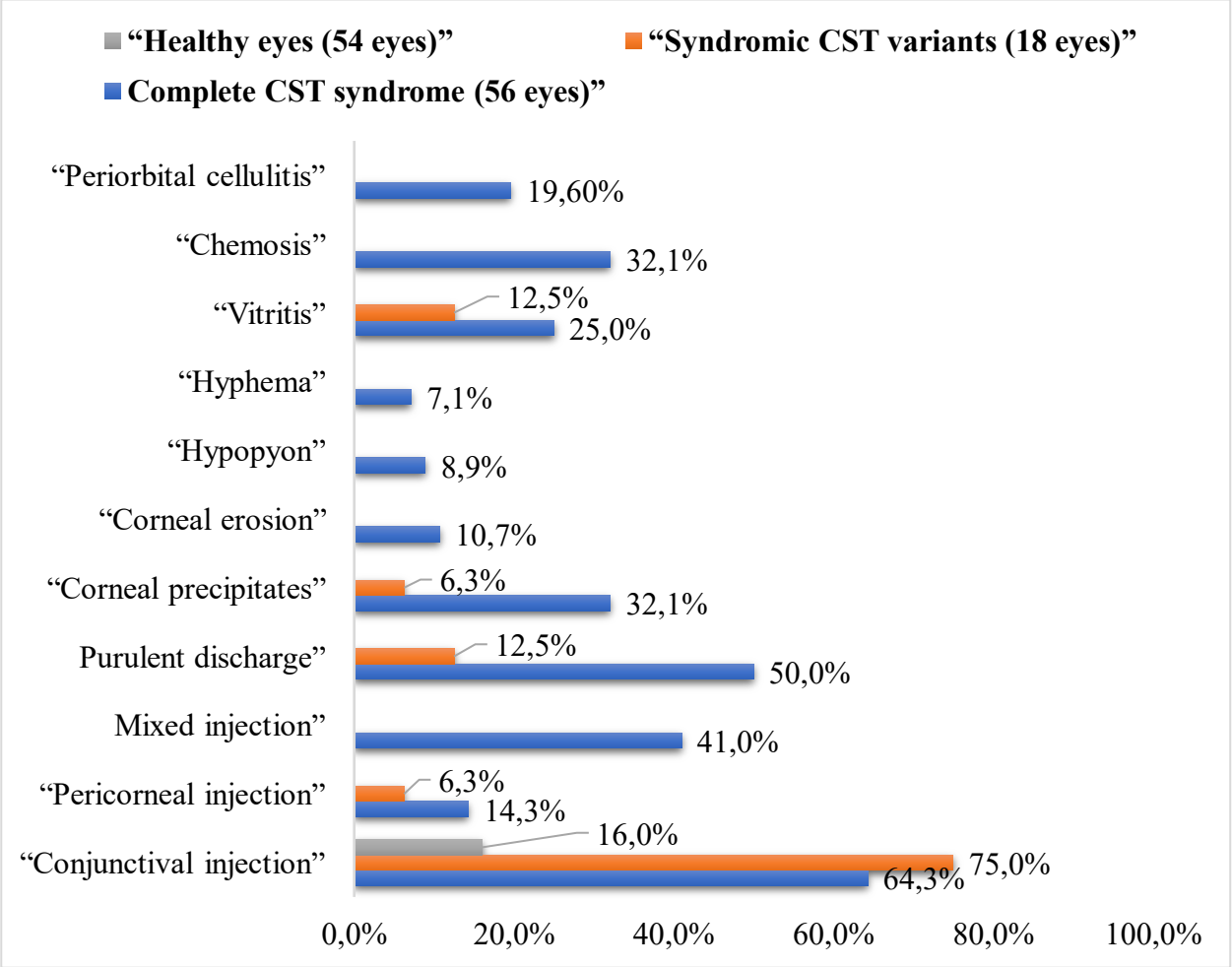

Figure 3.6. Prevalence of ophthalmological symptoms of inflammatory genesis.

Below are clinical examples of lesions of the eyeball structures in patients with COVID-19–associated CST (Fig. 3.7).

"Corneal precipitates" **"Uveitis"**

Endophthalmitis Panophthalmitis

“Figure 3.7. Clinical presentation of lesions of the eyeball structures in patients with COVID-19–associated CST.”

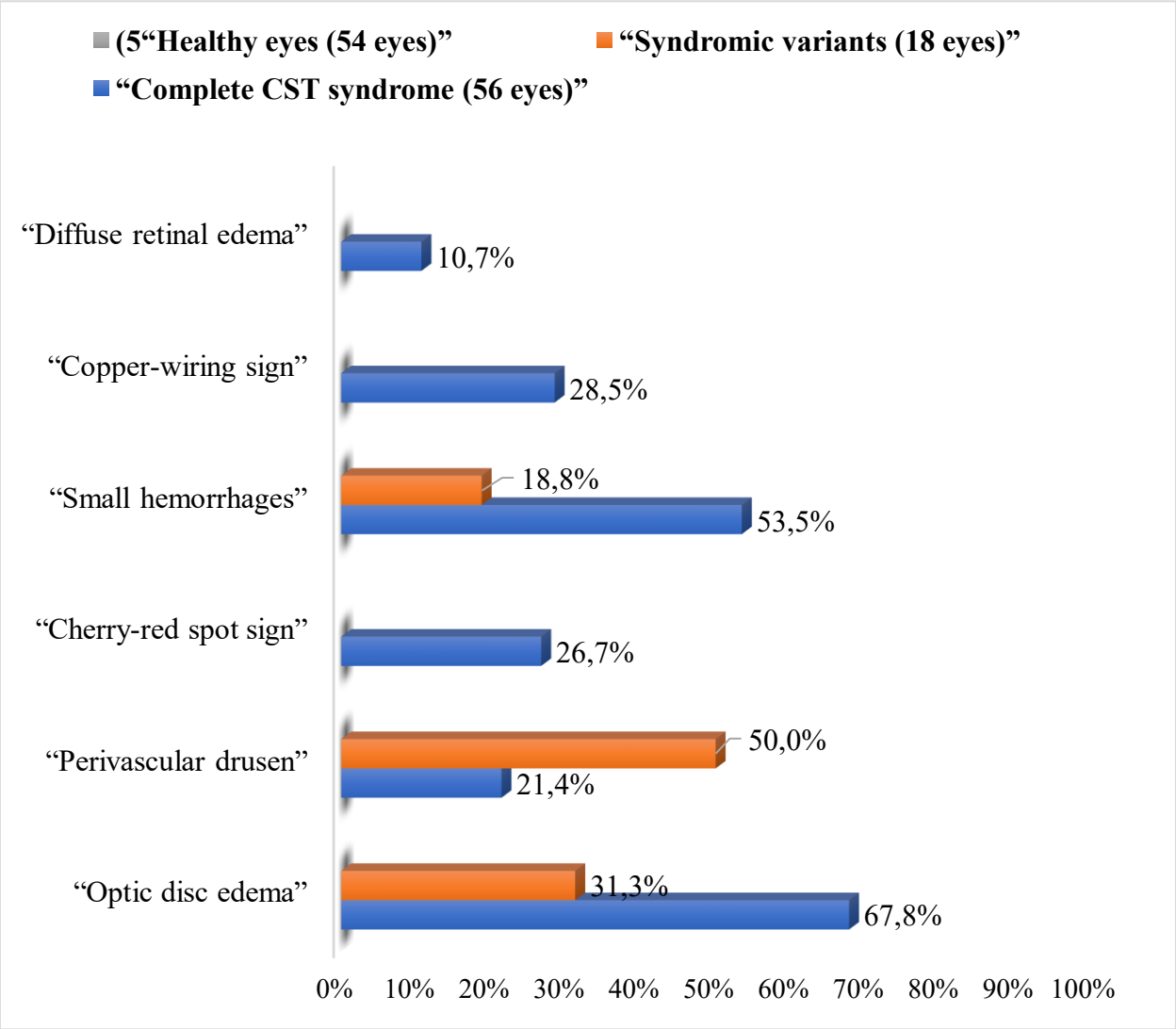

Figure 3.8. Ophthalmoscopic symptoms in patients with COVID-19–associated CST.

Figure 3.8 presents the results of the evaluation of specific fundus changes identified using ophthalmoscopy. In the eyes of patients with complete CST, the most common findings included optic disc edema, small hemorrhages, and pronounced signs of retinal ischemia manifested as the copper-wiring sign and the cherry-red spot. In eyes with incomplete cavernous sinus thrombosis, the most frequently observed changes were small hemorrhages and perivascular drusen (Fig. 3.9).

Optic disc edema **Multiple perivascular drusen**

“Signs of angiosclerosis (copper-wiring sign)” **“Signs of severe retinal ischemia (cherry-red spot sign)”**

Figure 3.9. Characteristic ophthalmoscopic signs in eyes with COVID-19–associated CST.

Fundus ophthalmoscopy was successfully performed in 75% of eyes with complete CST. In the remaining cases, examination was not possible due to the presence of vitritis, hypopyon, or pronounced corneal edema. Ophthalmoscopy revealed the following signs: optic disc edema (67.8%); presence of perivascular drusen (21.4%); cherry-red spot sign (26.7%), which was more frequently observed in patients during the convalescent phase; small hemorrhages in the equatorial region (53.5%); copper-wiring sign (28.5%); and diffuse retinal edema (10.7%).

Fundus ophthalmoscopy was successfully performed in 87.5% of eyes with syndromic variants of CST. The following signs were identified: optic disc edema (31.3%); presence of **perivascular drusen (50%); and small equatorial hemorrhages (18.8%).**

§ 3.3. Results of the assessment of the choroidal status using OCT

At the second stage of the study, we performed an evaluation of ocular structural involvement using optical coherence tomography (OCT), which enables assessment of morphological changes in cross-sectional scans of any retinal region, and OCT angiography, which allows visualization of the retinal vascular network at any layer without the use of contrast agents.

Figure 3.10. OCT and OCT-angiography findings.

Since retinal and optic nerve changes that develop as a result of CST are not specific, the main focus of our study was directed toward the evaluation of the choroid. This approach was also justified by multiple studies confirming the presence of systemic vasculitis in COVID-19, which could manifest as alterations in the thickness and structural characteristics of the choroid.

Using OCT, an assessment of choroidal thickness was performed in eyes with CST and in the healthy fellow eyes of the same patients. The results demonstrated that eyes with the complete variant of CST exhibited marked choroidal thickening. Eyes with partial (syndromic) CST also showed pronounced thickening. It is noteworthy that even in the healthy eyes of these patients, the mean choroidal thickness values were significantly higher than normal reference values.

“Figure 3.11. Method for assessing choroidal thickness.”

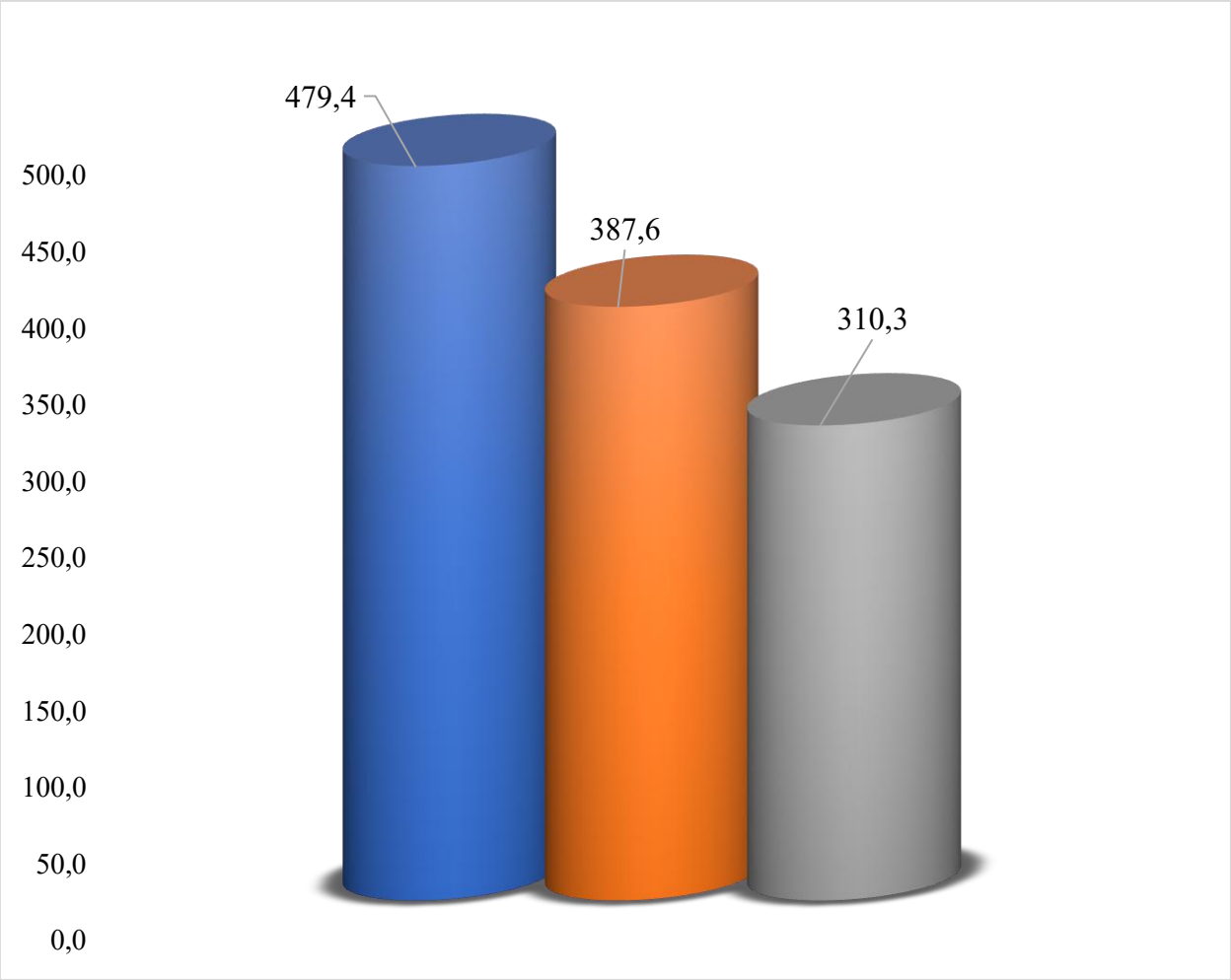

Figure 3.12. Comparative assessment of choroidal thickness, µm.

During the acquisition and analysis of angiographic findings in patients with severe disease, a reduction in the mean capillary network density was identified, primarily in the superficial vascular plexuses, across the entire inferior parafoveal and perifoveal segments. Focal segmentations and vascular narrowing

were also detected. The capillary diameter was reduced, the fan-shaped vascular pattern was disrupted, and the mean vascular density was decreased. However, in the peripapillary region, the anatomy and patency of the vessels in all vascular plexuses remained unchanged. The outer plexuses and the choriocapillaris layer showed no vascular abnormalities. A clinically significant finding was the pathological thickening of all layers of the choroid, including the choriocapillaris, Sattler's medium-vessel layer, and Haller's large-vessel layer.

In our study, we measured the subfoveal choroidal thickness on a horizontal scan passing through the center of the foveola. This distance is measured from the outer border of the retinal pigment epithelium to the inner border of the sclera in this region.

§ 3.4. Results of orbital structure assessment in patients with COVID-19–associated CST based on MRI findings

To evaluate orbital involvement, we used MRI in T2 TSE and Dark Fluid T2 modes with thin slices (0.6–1.6 mm), previously proposed by Bilalov, Umarov, and Oripov for early diagnosis of COVID-19–associated CST. The method is based on the detection of early CST signs manifested as changes within the orbital soft tissues.

Using this method, the following signs of orbital structural damage were identified:

- edema of para- and retrobulbar fat tissue;
- dilation of the superior ophthalmic vein with T2 signal enhancement;
- edema of extraocular muscles;
- anterior displacement of the eyeball;
- heterogeneous signal intensity of the cavernous sinus with hypointense areas on T2;
- enlargement of the cavernous sinus projection;

- enlargement of the optic nerve projection and the perineural subarachnoid space.

“In the right orbit, an enlargement of the extraocular muscle projections is observed as a result of their edema.	“In the right orbit, an enlargement of the projection of the superior ophthalmic vein is noted, resulting from a congestive process.”.
“In the left orbit, there is marked edema of the orbital soft-tissue structures accompanied by pronounced exophthalmos.”	“In the left orbit, an enlargement of the optic nerve projection is observed, resulting from its edema.”.

.

“Figure 3.13. Clinical examples of orbital structural alterations on MRI images.”

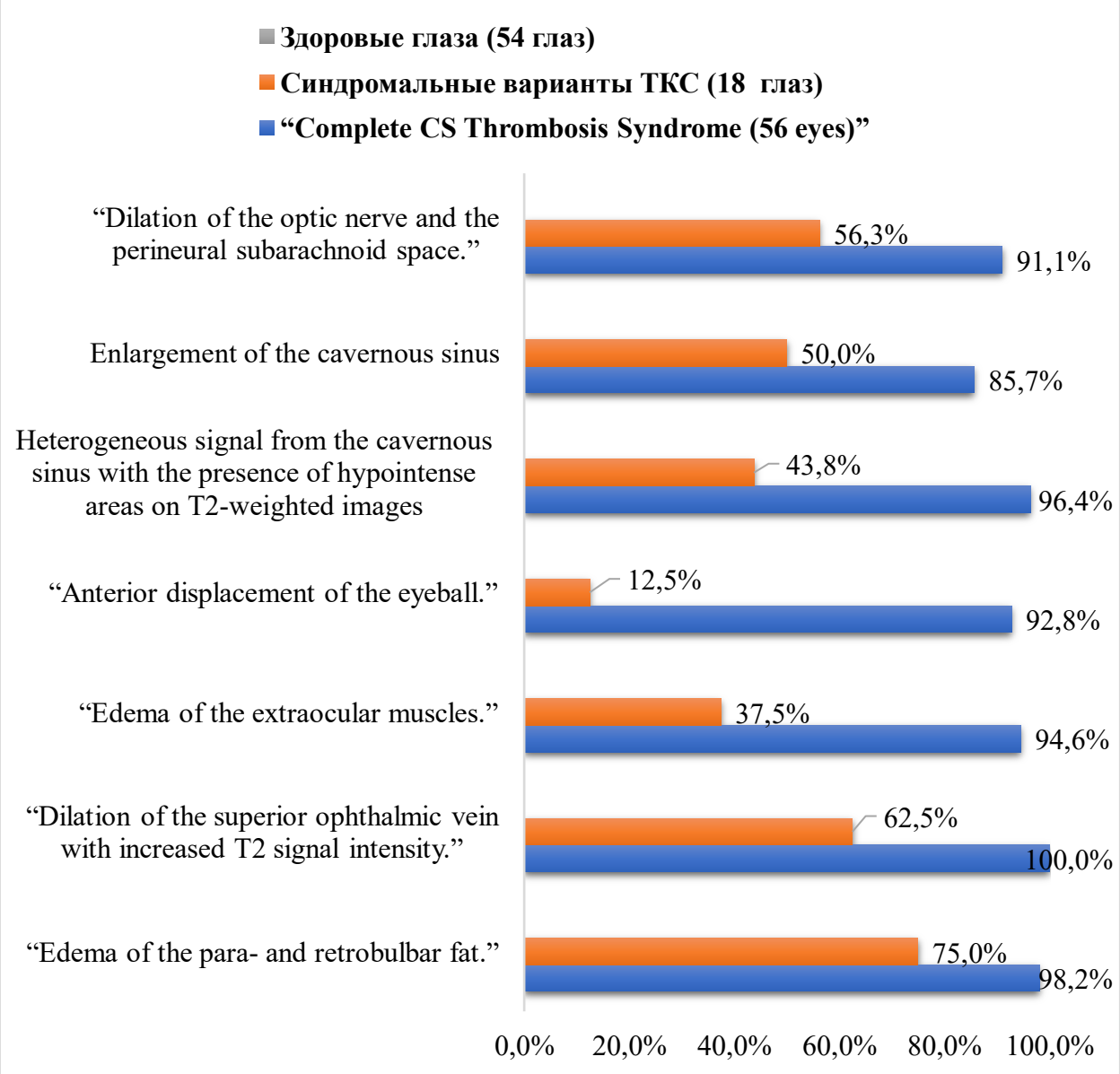

Figure 3.14. Prevalence of MRI signs of orbital involvement. Graph 3.14 shows the frequency of the indicated orbital involvement signs in complete and incomplete forms of cavernous sinus thrombosis (CST). It should be noted that in the syndromic variants of CST, signs of orbital soft-tissue involvement are also detected in an average of 65% of cases. This indicates that despite the absence of severe functional impairments, patients still exhibit edema of the parabular and retrobulbar fat, extraocular muscles, the optic nerve and its soft sheath, as well as venous congestion in the superior ophthalmic vein.

Figure 3.15. Clinical presentation of orbital bone involvement on MSCT.

Figure 3.15 demonstrates the pattern of orbital bone involvement in COVID-19–associated CST. Bone structures of the orbit were most frequently affected in the setting of a purulent-necrotic process, i.e., in cases of orbital phlegmon. In such cases, the process most commonly began with necrotic involvement of the medial orbital wall, where a defect subsequently formed, leading to the development of a pathological communication with the ethmoidal sinus. The presented images illustrate examples of a purulent-necrotic process accompanied by disruption of the bony wall’s integrity.

.

CHAPTER IV. RESULTS OF PATHOMORPHOLOGICAL EXAMINATION

As is well known, two variants of clinical presentation can be distinguished in cavernous sinus thrombosis (CST), each following certain characteristic patterns: an aseptic (ischemic) variant, characterized by a slow progression of symptoms, and a septic variant, in which symptoms appear abruptly and rapidly worsen. Analysis of classical archival cases showed that the septic variant was observed in 70% of cases, whereas the aseptic variant was present in 30%, and these two forms could be clearly differentiated based on their clinical manifestations. Damage to the endothelium of cerebral venous sinuses caused by the COVID-19 pathogen leads to the formation of platelet aggregates. This process results in thrombosis within the venous vessels of the brain. Early symptoms include headache, loss of consciousness, and seizures. From an ophthalmologic perspective, eyelid and ocular edema, redness, and tenderness are observed, followed by the development of exophthalmos. Among the possible complications are cerebral infarction and stroke. Cavernous sinus thrombosis represents an occlusion of the lumen of the cavernous sinus by a thrombus.

During the autopsy of a patient who died from COVID-19–associated CST, pathological material (fragments of the cavernous sinus and cerebral vessels) was obtained for the purpose of identifying the morphological basis of thrombogenesis. The conclusions of the pathomorphological analysis of cerebral vessels are presented below.

Pathomorphological examination revealed that some vessels exhibited endothelial injury with detachment and exposure of the basement membrane. The micrograph demonstrates the marginal arrangement of blood elements within the vessel lumen, characterized by cellular adhesion and infiltration of the vessel wall by leukocytes and lymphoid cells (Fig. 4.1).

In small cerebral vessels, fibrin strands were found within the lumen, forming a dense network that occluded the vessel in a segmental pattern (Fig. 4.2). Venous vessels exhibited pronounced stasis and erythrocyte sludging (Fig. 4.3),

accompanied by thinning of the vascular wall and marked perivascular edema of the brain parenchyma.

Figure 4.1. Marginal arrangement and adhesion of blood elements to the vascular wall. Staining: H&E. Magnification: 10×40.

Figure 4.2. Formation of a fibrin thrombus in the lumen of an arteriole. Staining: H&E. Magnification: 10×40.

Figure 4.3. Formation of an erythrocyte thrombus in the lumen of a venule. Staining: H&E. Magnification: 10×40.

Figure 4.4. Formation of an occlusive thrombus in the lumen of an arteriole. Staining: H&E. Magnification: 10×40.

Following coronavirus infection, coagulopathy develops in the cerebral vessels in the form of thrombus formation (fibrin–platelet thrombi in arterial lumens (Fig. 4.4), erythrocyte thrombi in venous vessels, and hyaline thrombi in capillaries). As a result of coagulopathy and thrombus formation in vessels of various calibers, the brain parenchyma develops edema, encephalomalacia, and perivascular cerebral infarctions.

Based on the pathological findings, it can be concluded that coronavirus infection affects the vascular system of the body. In particular, nearly all components of the vascular system in the cerebral vessels are involved. Initially, the endothelium is affected: due to viremia and toxemia, endothelial surface damage occurs, characterized by dystrophic swelling of the cytoplasm followed by detachment and exposure of the basal membrane. Subsequently, the basal and elastic membranes, the muscular layer, and the adventitia of the vessel wall become involved. Endothelial injury ultimately leads to thrombus formation.

§ 4.2. Results of the pathomorphological examination of orbital bone fragments and soft tissues

SARS-CoV-2, the virus that causes COVID-19, affects the angiotensin-converting enzyme 2 (ACE2) receptors expressed in the epithelium of the upper respiratory tract, alveolar cells, alveolar monocytes, vascular endothelium, salivary gland

epithelium, esophageal epithelium, macrophages, and various other cells that possess receptors for this virus, demonstrating its pronounced *polytropism*.

SARS-CoV-2 is capable of active replication in the epithelial cells of the upper respiratory tract. As a result, COVID-19 frequently presents with severe disease progression characterized by acute respiratory distress syndrome (ARDS). This severity is attributed to extensive viral replication in the bloodstream, immune system dysfunction, hypoxia, and multiorgan damage involving the heart, kidneys, lungs, esophagus, brain, and vascular system.

Expression of ACE2 receptors increases in the cells of various organs, leading to more severe disease approximately two weeks after infection. The pathogenesis of COVID-19 is defined by destructive–proliferative thrombovasculitis, hypercoagulation, microangiopathy, and immune system dysfunction.

Patients develop a hyperergic immune response to SARS-CoV-2 infection, resulting in a systemic inflammatory process involving the alveolar capillaries, severe damage to other organs, and the possible development of septic shock.

The pathogenic and morphogenetic aspects of COVID-19 described above remain insufficiently studied, particularly concerning areas rich in venous structures—such as the cerebral venous sinuses, facial veins, nasal cavity, paranasal sinuses, and orbital vasculature. In the tissues of these anatomical regions, thrombovasculitis and hypercoagulation syndrome lead to necrotic changes and inflammatory processes in the soft tissues.

Material for the pathomorphological analysis was obtained during surgical intervention. The specimens consisted of fragments of the ethmoid and maxillary bones, as well as orbital soft tissues. For morphological study, the material was fixed in a 10% neutral buffered formalin solution for three days. Following fixation, the tissue was rinsed in running water for at least two hours, dehydrated in alcohols of increasing concentration and chloroform, and subsequently embedded in paraffin wax.

Photographs of the prepared microscopic specimens and their descriptions are presented in Figure 4.5.

Figure 4.5 (A). Fragments of the ethmoid bone (medial orbital wall) showing resorption and calcification.

Figure 4.5 (B). Fragments of the ethmoid bone (medial orbital wall) containing an inflammatory infiltrate.

Figure 4.5 (C). Fragments of the ethmoid bone (medial orbital wall) with extensive hemorrhages.

Figure 4.5 (D). Marked edema and destructive changes are observed in the soft tissues of the orbit; the sinusoids are filled with mucus and exudate.

Figure 4.5 (E). Within the soft tissues, there are foci of inflammatory granulation tissue containing thin-walled blood vessels.

Figure 4.5 (D). Within the soft tissues, there are foci of inflammatory granulation tissue with fibrinoid necrosis of their walls and fibrin thrombi in the lumen.

As is well known, two variants of clinical presentation can be distinguished in cavernous sinus thrombosis (CST), each following certain characteristic patterns: an aseptic (ischemic) variant, characterized by a slow progression of symptoms, and a septic variant, in which symptoms appear abruptly and rapidly worsen. Analysis of classical archival cases showed that the septic variant was observed in 70% of cases, whereas the aseptic variant was present in 30%, and these two forms could be clearly differentiated based on their clinical manifestations.

Another important alteration consisted of pronounced tissue edema, leading to atrophy and disintegration of structural elements, while focal areas demonstrated necrobiosis. Observations showed that the pigment cells of the pigmented epithelium underwent atrophy and displacement, with some exhibiting degeneration and necrobiosis. In the anterior margin of the connective-tissue layer of the pigmented epithelium, coronavirus-induced changes included signs of mucoid and fibrinoid swelling within stromal vessels. The choroid occupies a large area of the eye and includes the iris, ciliary body, and choroidea. It is supplied by the posterior ciliary arteries, while the venous drainage system has a

specific structure, with a large volume of blood passing through varicose-like dilated veins, leading to frequent blood stasis. This, in turn, results in the retention of microorganisms along with blood, creating conditions for the development of inflammatory processes. Surrounding the choroidal capillaries is Bruch's membrane and a single layer of pigment epithelium, which separates the choroid from the retina. The choroid is not firmly fused with the sclera, which often leads to hemorrhages forming between them.

The choroid consists of five layers:

In the middle mesodermal layer, which is rich in blood vessels, pronounced circulatory disturbances were identified—namely venous hyperemia and hemorrhage. In the posterior pigment–muscle layer, pigment cells were found to be destroyed and fragmented, while muscle cells were in a state of involuntary contraction.

In some cases, lymphoproliferative immunopathological inflammation developed within the pigmented epithelium. A dense lymphoid infiltrate appeared in the anterior connective-tissue layer of the pigmented epithelium around the interstitial tissues and vessels. Lymphoid infiltrates were found predominantly around blood vessels, and lymphocytic thrombi were observed in some veins.

Microscopic examination of the pigmented epithelium, which forms part of the uveal tract, revealed several abnormalities, the most notable of which were pronounced vascular dilation, vascular congestion, and extravasation of blood into surrounding tissues (see Fig. 4.9).

In the middle mesodermal layer, rich in vessels, significant circulatory disturbances such as venous hyperemia and hemorrhage were detected. In the posterior pigment–muscle layer, pigment cells were destroyed and fragmented, and muscle cells were in a state of involuntary contraction. In several cases, lymphoproliferative immunopathological inflammation was noted within the pigmented epithelium. A dense lymphoid infiltrate was identified in the anterior connective-tissue layer surrounding interstitial tissues and vessels. These infiltrates were predominantly perivascular, and lymphocytic thrombi were

observed in several veins (Fig. 4.10). Lymphoid infiltrates mainly formed around the blood vessels, and lymphocytic thrombi developed in some veins.

§ 4.3. Pathomorphological findings of the ocular structures

In this study, tissues of the ocular globe were examined. The collected material included conjunctival tissue, cornea, sclera, choroidal vessels, iris, ciliary body, optic nerve, and retina.

Microscopic evaluation of the ocular structures in COVID-19–associated CST revealed various pathological changes, including circulatory disturbances, thrombosis, degeneration, and signs of inflammation.

4.3.1. Choroid

The choroid occupies a large area of the eye and includes the iris, ciliary body, and choroidea. It is supplied by the posterior ciliary arteries, while the venous drainage system has a specific structure, with a large volume of blood passing through varicose-like dilated veins, leading to frequent blood stasis. This, in turn, results in the retention of microorganisms along with blood, creating conditions for the development of inflammatory processes. Surrounding the choroidal capillaries is Bruch's membrane and a single layer of pigment epithelium, which separates the choroid from the retina. The choroid is not firmly fused with the sclera, which often leads to hemorrhages forming between them.

The choroid consists of five layers:

1. **Outer layer** – connective tissue attached to the sclera
2. **Layer of large vessels (Haller's layer)** – composed mainly of venous vessels
3. **Arterial layer of medium-sized vessels (Sattler's layer)**
4. **Choriocapillaris layer**
5. **Bruch's membrane**,
6. 2–3 μm thick, separating the choroid from the retina

In the choroidal tissue, numerous thrombi were identified in venous vessels traversing the sclera. The veins were paralytically dilated; their lumina contained

thrombi (Fig. 4.6), dense fibrin clots filling the lumen, desquamation of endothelial cells, lymphoid cells, and fragments of destroyed cells. The presence of lymphocytic thrombi in the veins confirms SARS-CoV-2 infection. As a result, the choroidal tissue exhibited dystrophic and necrobiotic alterations. Significant scleral thickening was also noted, indicating the development of acute edema.

Figure 4.6. Fragment of the border zone between the sclera and the choroid; fibrin and lymphocytic thrombi are identified within the lumen of the vein. Staining: H&E. Magnification: 10×40.

The pigment epithelium located beneath the choroid exhibited dystrophy and destruction, while the choriocapillaris vessels above it were dilated, resulting in slowed blood inflow. The arterial blood vessels were also slightly dilated, and the veins appeared more lucent; some were filled with erythrocytes, whereas others contained plasma (Fig. 4.7), which indicated altered hemodynamics in the atrophic tissues.

When the choroid was affected by the coronavirus, an immunopathological reaction developed, characterized by the formation of a lymphoproliferative infiltrate as a result of acute autoimmune injury within its tissues (Fig. 4.8).

Figure 4.7. The uveal tract of the eyeball showing pronounced signs of circulatory disturbances, interstitial tissue edema, and tissue dystrophy and necrobiosis. Staining: H&E. Magnification: 10×40..

Figure 4.8. The uveal tract of the eyeball showing lymphoid infiltration across all layers. Staining: H&E. Magnification:

From the vascular layers. Venous vessels within the venous layer were markedly dilated, some of them ruptured, with hemorrhages developing around them. Necrobiotic degeneration and necrosis were observed in the tissues located between the lymphoid infiltrates.

Since the pigment epithelium constitutes a component of the choroid, microscopic examination revealed the following changes, the most prominent of which were

marked dilation of blood vessels, their congestion with blood, and erythrodiapedesis.

Figure 4.9. Iris: marked vascular dilation, perivascular hemorrhages, tissue edema, and lymphoid infiltration of the interstitial tissue. Staining: H&E. Magnification: 10×40.

Another important alteration consisted of pronounced tissue edema, leading to atrophy and disintegration of structural elements, while focal areas demonstrated necrobiosis. Observations showed that the pigment cells of the pigmented epithelium underwent atrophy and displacement, with some exhibiting degeneration and necrobiosis. In the anterior margin of the connective-tissue layer of the pigmented epithelium, coronavirus-induced changes included signs of mucoid and fibrinoid swelling within stromal vessels.

In the middle mesodermal layer, which is rich in blood vessels, pronounced circulatory disturbances were identified—namely venous hyperemia and hemorrhage. In the posterior pigment–muscle layer, pigment cells were found to be destroyed and fragmented, while muscle cells were in a state of involuntary contraction.

In some cases, lymphoproliferative immunopathological inflammation developed within the pigmented epithelium. A dense lymphoid infiltrate appeared in the anterior connective-tissue layer of the pigmented epithelium around the interstitial tissues and vessels. Lymphoid infiltrates were found predominantly around blood vessels, and lymphocytic thrombi were observed in some veins.

Microscopic examination of the pigmented epithelium, which forms part of the uveal tract, revealed several abnormalities, the most notable of which were pronounced vascular dilation, vascular congestion, and extravasation of blood into surrounding tissues (see Fig. 4.9).

In the middle mesodermal layer, rich in vessels, significant circulatory disturbances such as venous hyperemia and hemorrhage were detected. In the posterior pigment–muscle layer, pigment cells were destroyed and fragmented, and muscle cells were in a state of involuntary contraction. In several cases,

lymphoproliferative immunopathological inflammation was noted within the pigmented epithelium. A dense lymphoid infiltrate was identified in the anterior connective-tissue layer surrounding interstitial tissues and vessels. These infiltrates were predominantly perivascular, and lymphocytic thrombi were observed in several veins (Fig. 4.10). Lymphoid infiltrates mainly formed around the blood vessels, and lymphocytic thrombi developed in some veins.

Figure 4.10. ***Iris: the outer and middle layers exhibit pronounced loose lymphoid infiltration.*** **Staining: H&E. Magnification: 10×40.**

Examination of the ciliary body revealed the development of marked circulatory, inflammatory, and destructive–necrotic alterations, which were most frequently identified on histological sections (see Fig. 4.11). The circulatory disturbances were characterized by dilation of blood vessels, tissue edema, and atrophy, accompanied by hemorrhages in certain areas.

Figure 4.11. ***Ciliary body: extensive hemorrhages, foci of edema, and tissue necrosis.*** **Staining: H&E. Magnification: 10×40.**

As a result, compression, deformation, and structural alterations were identified, leading to dystrophic and necrotic changes in some of the muscular lamellae of the ciliary body. The muscle fibers of the ciliary body were dilated and deformed; signs of mucoid and fibrinoid swelling, as well as necrosis, were detected within its stroma. Detachment of the ciliary body's basal membrane from the sclera and its deformation were also observed, caused by edema associated with fibrinoid swelling and fibrinoid necrosis.

In some cases, the mesodermal portion of the ciliary body exhibited predominant lymphoid infiltration and vascular atrophy (Fig. 4.12). As a result, signs of dystrophy and destruction of pigment cells within the ciliary body were identified.

Figure 4.12. ***Ciliary body: lymphoid infiltration in the mesodermal layer; pigment cells exhibit dystrophy and destruction.*** **Staining: H&E. Magnification: 10×40.**

4.3.2. Retina

In the course of studying the pathomorphological changes occurring in the ocular tissues as a result of SARS-CoV-2–related complications, special attention—following the vascular layer—was directed to the retina. It was established that in most cases, the retina became detached from the underlying choroid, accompanied by extensive hemorrhage. Within the surrounding blood, lymphoid cells were identified in addition to plasma cells and erythrocytes. The retina was found to be deformed and focally condensed in certain areas (Fig. 4.13).

It should be noted that in various cases of retinal involvement, severe hemorrhages were also detected within the choroid, along with profound tissue and cellular alterations leading to destruction and necrosis (Fig. 4.14).

Figure 4.13. ***Retina: complete detachment from the choroid with formation of a hemorrhage between them.*** **Staining: H&E. Magnification: 10×40.**

Figure 4.14. ***Retina: pronounced edema leading to vacuolization, loosening, and necrobiosis across all layers.*** **Staining: H&E. Magnification: 10×40.**

The choroid and the nuclear layers of the retina were also edematous, with destruction of cellular and tissue structures, resulting in a disruption of normal histotopography. Similar changes were observed in the outer plexiform and nuclear layers. The subsequent inner nuclear layer and internal limiting membrane showed deformed cell nuclei clustered into large accumulations. The ganglion cell layer was extensively damaged, with partial loss of neuronal cells, while the intercellular spaces became edematous and vacuolated. The outer limiting membrane was not identifiable, and the inner retinal layers were intermixed with blood, lacking any organized structural pattern (Fig. 4.15).

Figure 4.15. ***Retina: the ganglion cell layer and the internal limiting membrane have undergone destruction and atrophy, with tissues intermixed with blood elements.*** **Staining: H&E. Magnification: 10×40.**

4.3.3. Optic Nerve

During microscopic examination of the optic nerve, attention must be paid to its histotopographic architecture and structural composition. The nerve fibers

are surrounded by a thick outer sheath—the epineurium—and each nerve fiber is encased by the perineurium, which consists of specialized membranes containing sensory neuronal elements.

Microscopic evaluation of optic nerve fibers damaged as a result of venous sinus thrombosis of the brain in the context of COVID-19 revealed that the external epineurial sheath, composed of connective tissue and associated cells, was edematous and had lost its normal histotopography. Both within and outside this sheath, inflammatory infiltrates were present. Within the epineurium, areas of pronounced dilation of nerve fibers were observed (Fig. 4.16).

Figure 4.16. ***Optic nerve: marked edema within the epineurium, displacement of nerve fibers, and vacuolization of Schwann cells.***

Staining: H&E. Magnification: 10×40.

Each nerve fiber bundle within the perineurium, formed by specialized cells, demonstrated a reduction in volume due to dystrophic changes in the perineurial cells. Cytoplasmic edema was identified in each fiber bundle, indicating vacuolization. The nerve fibers were structurally damaged and deformed.

4.3.4. Fibrous Tunic

The sclera is a dense, tightly arranged, non-transparent outer coat of the eyeball. Externally, it is connected to the venous vessels via the episclera. The middle layer consists of fibrocytes and collagen fibers characteristic of the sclera. Within the coat lies a thin layer of blood vessels containing pigmented chromophore cells, which impart coloration to the structure.

Figure 4.17. ***Sclera: loosening of all layers due to edema. Necrobiosis and inflammatory infiltration.***

Staining: H&E. Magnification: 10×40.

Microscopic examination of scleral changes resulting from cavernous sinus thrombosis of the brain associated with COVID-19 revealed the following alterations. Destructive and inflammatory processes were predominantly

observed in all layers of the sclera (see Fig. 4.17). However, the outer coat—the episclera—was affected most severely. In this region, the episcleral vessels were markedly dilated, blood-filled, and showed signs of atrophy. This layer was completely infiltrated, with the infiltrates composed mainly of lymphocytes and histiocytes (Fig. 4.18).

Figure 4.18. ***Sclera: the episclera has undergone diffuse infiltration as a result of the inflammatory process.*** **Staining: H&E. Magnification: 10×40.**

Figure 4.19. ***Sclera: proliferation of lymphocytic cells is observed around the vascular wall.*** **Staining: H&E. Magnification: 10×40.**

The vascular walls of the episclera and the surrounding connective tissues also underwent changes associated with fibrinoid swelling and fibrinoid necrosis, as well as the formation of metachromatic inclusions containing glycosaminoglycans. The vascular walls were infiltrated by lymphoid cells and showed signs of atrophy (see Fig. 4.19).

The middle layer of the sclera, which contains fibrocytes and collagen fibers, also exhibited edema and deformation primarily due to swelling of the collagen fibers. The inner pigmented layer of the sclera likewise underwent changes, resulting in the dispersion of pigment granules within its matrix.

4.3.5. Cornea.

In cases of cavernous sinus thrombosis resulting from COVID-19, pathomorphological alterations were also identified in the cornea.

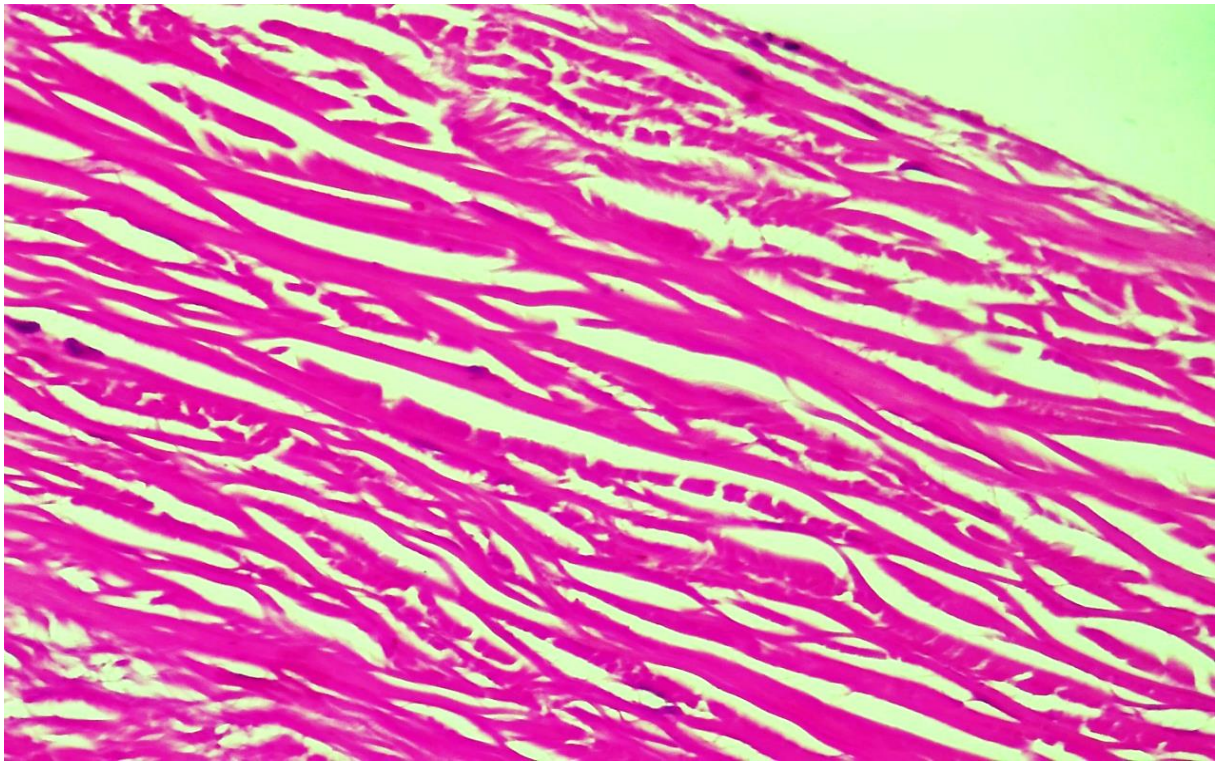

Figure 4.20. ***Cornea: detachment of the stratified squamous epithelium, stromal edema, loosening of collagen fibers.***

Staining: H&E. Magnification: 10×40.

These alterations included the following: the corneal epithelium became multilayered, the basal membrane was disrupted, and in some areas thick mucous and fibrinous deposits and deformities were observed along the basal membrane.

In the middle (stromal) layer of the cornea, thick collagen fibers were noted, some of which exhibited edema (Fig. 4.20), deformation, and enlargement. Additionally, the corneal epithelium showed loss of integrity across the entire surface, and the basal membrane was destroyed (Fig. 4.21).

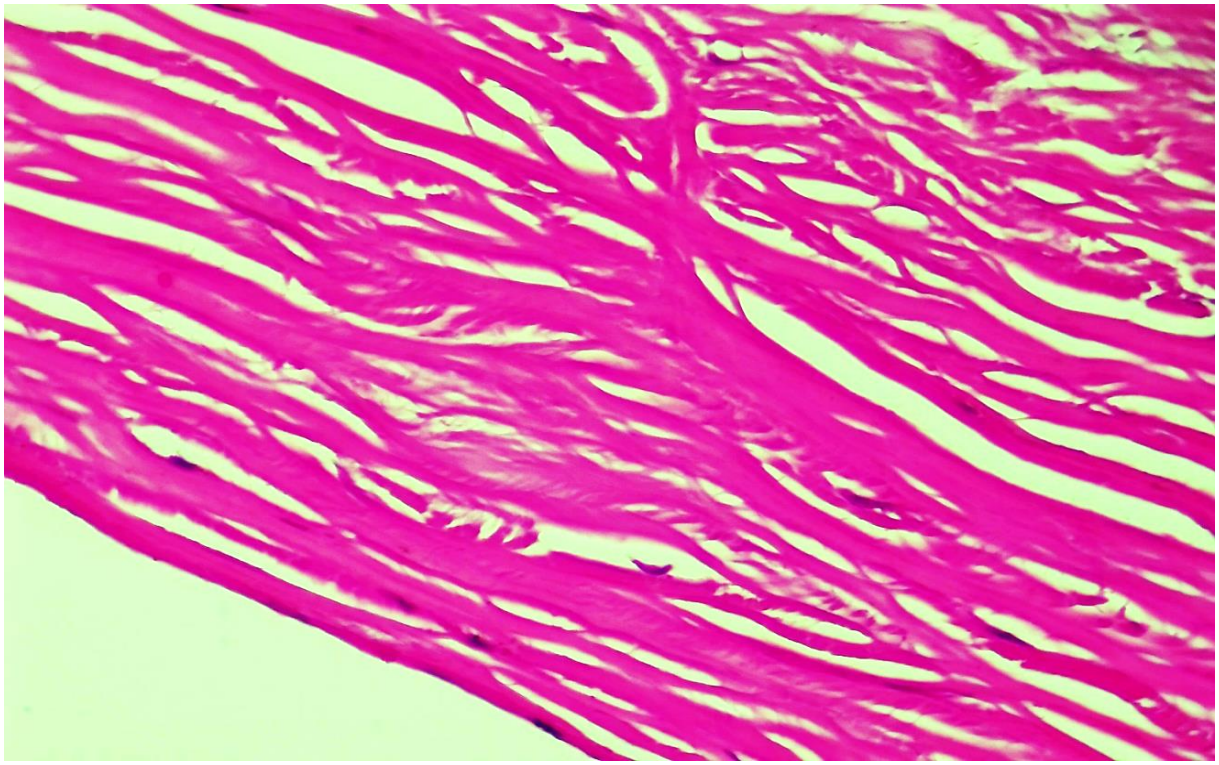

Figure 4.21. ***Cornea: epithelial detachment and stromal edema.*** **Staining: H&E. Magnification: 10×40.**

4.3.6. Conjunctiva

The conjunctiva is a multilayered mucous membrane that covers the surface of the eye and contains a specialized lamina that ensures conjunctival mobility. Beneath this lamina are located goblet cells.

In diseases associated with thrombosis of the cerebral venous sinuses resulting from COVID-19, various pathological alterations were identified in the conjunctiva, including changes related to circulatory disturbances and inflammatory processes. This process is characterized by a lymphoproliferative pattern and is primarily observed within the substantia propria.

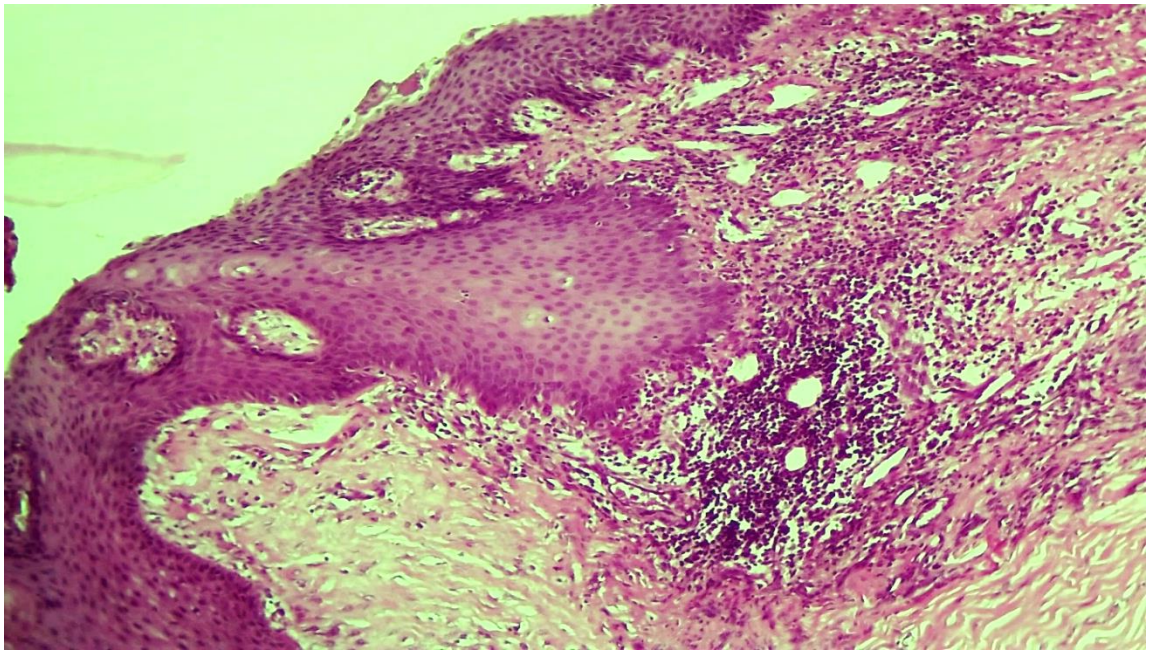

Figure 4.22. ***Conjunctiva: lymphoid infiltration of the substantia propria of the mucous membrane.*** **Staining: H&E. Magnification: 10×40.**

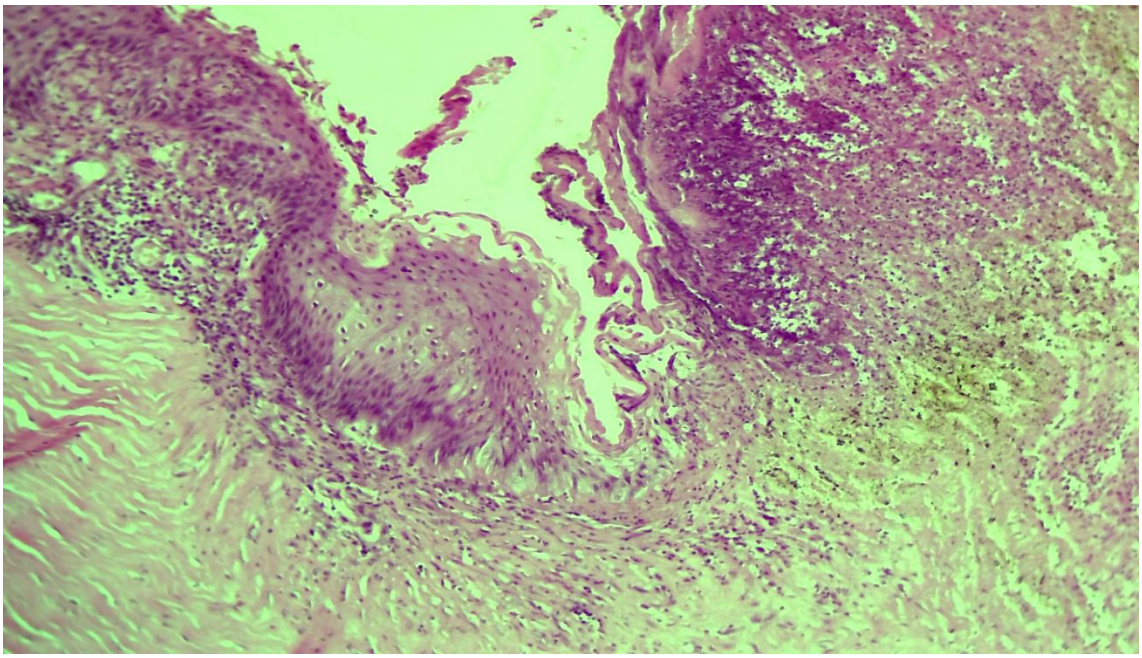

Figure 4.23. ***Conjunctiva: necrosis of the surface epithelium and the substantia propria.*** **Staining: H&E. Magnification: 10×40.**

There was proliferation of blood vessels and mucosal cells, along with lymphoid infiltration. In some areas, lymphoid infiltration appeared as well-formed lymphoid follicles (Fig. 4.22), while in other regions of the conjunctiva the infiltration by lymphocytes was less pronounced, particularly within the blood vessels. The conjunctival surface epithelium became multilayered due to acanthosis. Some cells showed cytoplasmic vacuolization. In certain cases, there

was intense lymphoid infiltration in the substantia propria, necrosis of tissue cells, and even necrosis of the epithelial covering on the surface (Fig. 4.23).

CONCLUSION

According to the available scientific literature, cavernous sinus thrombosis (CST) is considered one of the most severe complications associated with inflammatory disorders of various craniofacial regions, including the maxillofacial area, the orbit, the ear, the paranasal sinuses, and the oral cavity. Epidemiological data indicate that CST is rare, accounting for only 0.3–0.5% of all thrombotic complications. Over the past two decades, only isolated cases have been documented in major medical centers of developed European countries. Most publications consist of clinical case descriptions or small case series; large-scale clinical studies remain unavailable.

Despite the emergence of studies addressing CST in the context of COVID-19, current knowledge about the mechanisms and clinical course of COVID-19–associated CST remains limited. Several reports describe this complication during coronavirus infection, but a comprehensive investigation involving a large patient cohort has been conducted only in India. Those findings suggested that CST in COVID-19 patients may be associated with fungal infection—primarily mucormycosis. Based on this concept, CST may develop due to fungal invasion of the facial, orbital, and intracranial structures in the setting of COVID-19.

Given the relatively high incidence of CST among patients recovering from COVID-19 in our country, a series of studies addressing COVID-19–associated CST was initiated. These investigations included the first detailed evaluation of ophthalmic features of CST, the development of effective imaging approaches and surgical access to the orbit, and analysis of neuro-ophthalmic manifestations and necrotic complications involving facial structures in COVID-19–associated CST. However, it should be emphasized that histopathological studies of orbital tissues and ocular structures have not been previously conducted.

In light of the above, the considerable number of CST cases observed in our national clinical practice provides a solid basis for conducting an in-depth, comprehensive investigation of COVID-19–associated CST, including the morphological aspects of ocular involvement.

Aim of the Study pathological processes developing in the structures of the eyeball and its adnexa in COVID-19–associated cavernous sinus thrombosis.

Objectives To achieve the aim, the following objectives were formulated:

- to analyze the clinical patterns of inflammatory involvement of ocular structures in COVID-19–associated CST;
- to investigate the clinical and morphological features of purulent-inflammatory processes in orbital structures using MRI;
- to evaluate clinical and morphological changes in ocular tissues based on OCT and OCT-angiography findings;
- to provide a histopathological description of structural changes in orbital bones and soft tissues in COVID-19–associated CST;
- to determine the morphological characteristics of intraocular structures affected by COVID-19–associated CST.
- Another important alteration consisted of pronounced tissue edema, leading to atrophy and disintegration of structural elements, while focal areas demonstrated necrobiosis. Observations showed that the pigment cells of the pigmented epithelium underwent atrophy and displacement, with some exhibiting degeneration and necrobiosis. In the anterior margin of the connective-tissue layer of the pigmented epithelium, coronavirus-induced changes included signs of mucoid and fibrinoid swelling within stromal vessels.
- In the middle mesodermal layer, which is rich in blood vessels, pronounced circulatory disturbances were identified—namely venous hyperemia and hemorrhage. In the posterior pigment–muscle layer, pigment cells were found to be destroyed and fragmented, while muscle cells were in a state of involuntary contraction.

In some cases, lymphoproliferative immunopathological inflammation developed within the pigmented epithelium. A dense lymphoid infiltrate appeared in the anterior connective-tissue layer of the pigmented epithelium around the interstitial tissues and vessels. Lymphoid infiltrates were found predominantly around blood vessels, and lymphocytic thrombi were observed

in some veins. Microscopic examination of the pigmented epithelium, which forms part of the uveal tract, revealed several abnormalities, the most notable of which were pronounced vascular dilation, vascular congestion, and extravasation of blood into surrounding tissues (see Fig. 4.9).In the middle mesodermal layer, rich in vessels, significant circulatory disturbances such as venous hyperemia and hemorrhage were detected. In the posterior pigment–muscle layer, pigment cells were destroyed and fragmented, and muscle cells were in a state of involuntary contraction. In several cases, lymphoproliferative immunopathological inflammation was noted within the pigmented epithelium. A dense lymphoid infiltrate was identified in the anterior connective-tissue layer surrounding interstitial tissues and vessels. These infiltrates were predominantly perivascular, and lymphocytic thrombi were observed in several veins (Fig. 4.10). Lymphoid infiltrates mainly formed around the blood vessels, and lymphocytic thrombi developed in some veins.

MethodsThe diagnostic methods used in the study included: general ophthalmic examinations (visometry, ophthalmoscopy, biomicroscopy), advanced imaging techniques (optical coherence tomography and OCT-angiography), radiological methods (magnetic resonance imaging), and histopathological examination of tissue specimens.

The study consisted of three sequential stages.
At the **first stage**, the clinical characteristics of orbital and ocular involvement were evaluated.
At the **second stage**, structural changes in the orbit and the eyeball were assessed using advanced medical imaging methods.
At the **third stage**, histopathological examination was performed on specimens of orbital bone fragments, soft tissues, and ocular structures obtained during surgical intervention.

Clinical observations demonstrated that the analyzed cases of CST exhibited a distinctive and variable clinical course. These cases could not be unequivocally classified as either aseptic or septic. Some patients presented with a gradual progression of symptoms typical of aseptic thrombosis, whereas others

exhibited clinical signs consistent with orbital cellulitis, suggestive of septic CST. It remained challenging to determine the primary pathological event—whether purulent hemisinusitis spread to the orbit, or whether CST occurred first, subsequently complicated by necrotizing infection of the paranasal sinuses.

Subsequently, all eyes in the cohort (128 eyes) were randomized into three groups according to the form of pathological involvement:

1. complete CST syndrome,
2. syndromic variants of CST,
3. unaffected (healthy) eyes.

Analysis of the frequency of inflammatory manifestations in the orbit and the eyeball showed that **46%** of eyes with complete CST demonstrated infiltrative inflammation of orbital contents, confirmed by MRI. **Orbital phlegmon** was diagnosed in **17.8%** of eyes. Inflammatory disorders such as uveitis, endophthalmitis, and panophthalmitis were significantly less common. Importantly, none of these severe inflammatory manifestations were observed in eyes with syndromic variants of CST.

Because CST-related changes in the retina and optic nerve are generally nonspecific, the primary focus of this study was directed toward evaluating the **choroid**. This decision was further supported by mounting evidence of systemic vasculitis in COVID-19, which could manifest as alterations in the thickness and architecture of the choroid. Using OCT, choroidal thickness was measured in CST-affected and contralateral healthy eyes of the same patients. The results demonstrated marked choroidal thickening in eyes with complete CST. Eyes with partial syndromic variants also showed significant thickening. Notably, even in clinically healthy eyes of the same patients, mean choroidal thickness values were significantly higher than reference norms.

OCT-angiography in patients with severe CST revealed a reduction in the density of the superficial capillary plexus, predominantly affecting the inferior parafoveal and perifoveal sectors. Focal segmentations and narrowing of the vascular network were observed. Capillary diameter was reduced, the normal radial vascular pattern was disrupted, and overall vessel density was decreased.

Nevertheless, in the peripapillary region, vascular anatomy and perfusion remained preserved across all plexuses. No abnormalities were detected in the choriocapillaris or deeper choroidal layers. A clinically significant finding was the pathological thickening of all choroidal layers, including the choriocapillaris, Sattler's layer, and Haller's layer.

It should also be emphasized that syndromic CST variants exhibited signs of orbital soft-tissue involvement in approximately **65%** of cases. This indicates that, despite the absence of profound functional impairment, patients frequently presented with edema of the parabular and retrobulbar fat, extraocular muscles, the optic nerve and its sheath, as well as venous congestion of the superior ophthalmic vein.

The bony structures of the orbit were most commonly affected in cases complicated by a purulent-necrotic process—namely, orbital phlegmon. Typically, the process began with necrotic destruction of the **medial orbital wall**, which subsequently developed a structural defect, forming an abnormal communication with the ethmoidal sinus. The provided imaging examples demonstrate progressive necrotizing involvement with loss of continuity of the orbital bone.

During the Another important alteration consisted of pronounced tissue edema, leading to atrophy and disintegration of structural elements, while focal areas demonstrated necrobiosis. Observations showed that the pigment cells of the pigmented epithelium underwent atrophy and displacement, with some exhibiting degeneration and necrobiosis. In the anterior margin of the connective-tissue layer of the pigmented epithelium, coronavirus-induced changes included signs of mucoid and fibrinoid swelling within stromal vessels.

In the middle mesodermal layer, which is rich in blood vessels, pronounced circulatory disturbances were identified—namely venous hyperemia and hemorrhage. In the posterior pigment–muscle layer, pigment cells were found to be destroyed and fragmented, while muscle cells were in a state of involuntary contraction.

In some cases, lymphoproliferative immunopathological inflammation developed within the pigmented epithelium. A dense lymphoid infiltrate appeared in the anterior connective-tissue layer of the pigmented epithelium around the interstitial tissues and vessels. Lymphoid infiltrates were found predominantly around blood vessels, and lymphocytic thrombi were observed in some veins.

Microscopic examination of the pigmented epithelium, which forms part of the uveal tract, revealed several abnormalities, the most notable of which were pronounced vascular dilation, vascular congestion, and extravasation of blood into surrounding tissues (see Fig. 4.9).

In the middle mesodermal layer, rich in vessels, significant circulatory disturbances such as venous hyperemia and hemorrhage were detected. In the posterior pigment–muscle layer, pigment cells were destroyed and fragmented, and muscle cells were in a state of involuntary contraction. In several cases, lymphoproliferative immunopathological inflammation was noted within the pigmented epithelium. A dense lymphoid infiltrate was identified in the anterior connective-tissue layer surrounding interstitial tissues and vessels. These infiltrates were predominantly perivascular, and lymphocytic thrombi were observed in several veins (Fig. 4.10). Lymphoid infiltrates mainly formed around the blood vessels, and lymphocytic thrombi developed in some veins.

Histopathological analysis demonstrated that COVID-19 produces widespread vascular injury throughout the body. In the cerebral vasculature, virtually all structural components of the vascular system were affected. The earliest pathological change involved endothelial damage: viral dissemination (viremia) and toxin-mediated injury led to cytoplasmic swelling of endothelial cells, followed by their detachment and exposure of the underlying basement membrane. Subsequently, the basement membrane, elastic lamina, smooth-muscle layer, and adventitia became involved. Endothelial destruction triggered active intravascular thrombogenesis.

Additional material for histopathological assessment consisted of fragments of the ethmoid and maxillary bones as well as soft tissues of the orbit. These samples

were obtained during surgical intervention. consistent with the findings of this study.

The present investigation also included ocular tissues: conjunctiva, cornea, sclera, choroidal vessels, iris, ciliary body, optic nerve, and retina. Microscopy of ocular structures in COVID-19–associated CST revealed multiple pathological changes, including circulatory disturbances, thrombosis, cellular injury, and inflammatory reactions.

In the choroid, numerous venous thrombi were identified in vessels traversing the sclera. The veins were markedly dilated and filled with dense fibrin clots accompanied by endothelial desquamation, lymphoid elements, and fragmented cellular debris. The presence of lymphocytic thrombi strongly supported a viral etiology. Choroidal tissues showed pronounced dystrophic and necrobiotic changes. Significant thickening of the sclera was also noted, reflecting acute edema. Exposure of the choroid to SARS-CoV-2 initiated a pronounced immune-mediated response characterized by lymphoproliferative infiltration secondary to acute autoimmune-like tissue injury.

The choroid and nuclear layers of the retina exhibited edema, and the architecture of cellular layers was severely disrupted, compromising normal histotopography. Similar degenerative alterations were present in synaptic and nuclear layers. The inner nuclear layer and internal limiting membrane demonstrated clusters of deformed nuclei. The ganglion cell layer was destroyed, neuronal elements were partially lost, and the intervening spaces showed edema and vacuolization. The internal limiting membrane was no longer discernible, and retinal layers were intermixed with extravasated blood without structural organization.

Microscopic examination of the optic nerve emphasized assessment of its histotopographic arrangement. Nerve fibers are normally surrounded by a dense epineurial sheath, and each fiber is enclosed by perineurial layers composed of specialized supportive cells. In CST-related optic nerve injury, the epineurium exhibited severe edema, loss of structural organization, and infiltration both within and around the sheath. Pronounced dilation of nerve fiber bundles was

observed within the epineurium, reflecting significant axonal and Schwann-cell injury.

CONCLUSIONS

1. The clinical features of the inflammatory process in ocular structures in COVID-19–associated cavernous sinus thrombosis (CST) are characterized by pronounced polymorphism, with predominant involvement of the choroidal vasculature and retinal layers.

2. Orbital involvement in COVID-19–associated CST is marked by early manifestations of infiltrative inflammation and soft-tissue edema—observed in more than 90% of eyes with the complete CST syndrome and in more than 50% of eyes with syndromic variants, according to MRI findings.

3. It was established that COVID-19–associated CST leads to a significant thickening of all choroidal layers ($p < 0.05$) in eyes with the complete CST syndrome and its syndromic variants (479.4 μm and 387.6 μm, respectively, on OCT). Vascular angioarchitecture demonstrated loosening and structural disorganization. Importantly, choroidal thickening was also identified in clinically unaffected, contralateral eyes (310.3 μm), indicating that the emerging pachychoroidal vasculopathy reflects a systemic pathological process.

4. Histopathological analysis of ocular tissues demonstrated that COVID-19–associated CST induces a specific inflammatory response within the vascular walls of the choroid, iris, and ciliary body, characterized by the formation of lymphocytic thrombi. These changes promote further circulatory disturbances, edema, and necrobiotic degeneration across all structures interconnected with the uveal tract.

PRACTICAL RECOMMENDATIONS

1. It is recommended to apply the presented clinical description and semiotic profile of inflammatory lesions of the eyeball in patients with COVID-19–associated cavernous sinus thrombosis during routine clinical assessment of individuals presenting with this complication.
2. It is advisable to perform continuous clinical monitoring of the fellow, ostensibly healthy eye, with particular attention to the condition of the choroid and retina, in patients diagnosed with COVID-19–associated cavernous sinus thrombosis.
3. It is recommended to incorporate MRI findings when evaluating the likelihood of infiltrative inflammation and/or soft-tissue orbital edema in cases of syndromic variants of partial cavernous sinus thrombosis associated with COVID-19.

LIST OF REFERENCES

1.	Abdulkerimov Kh.T., Nagovitsyn I.A., Tarasevich T.N., Velikhanova M.S. Pathogenetic mechanisms and modern approaches to the treatment of inflammatory diseases of the paranasal sinuses. Russian Rhinology. 2012; (2):33.
2.	Aznabaeva LF. Pro-inflammatory cytokines in the immunopathogenesis and treatment of chronic purulent rhinosinusitis. [Abstract of Dissertation for the Degree of Doctor of Medical Sciences]. Saint Petersburg; 2022. 38 p.
3.	Sidorenko I.V. Local immunity factors and microflora in the development of chronic sinusitis.In: Proceedings of the Russian Scientific and Practical Conference "Experience in Therapeutic Practice and Training in Otorhinolaryngology."Vestnik Otorinolaringologii. 2023; p. 79–80.
4.	Aznabaeva L.F., Arefyeva N.A., Salakhova A.Kh *Cytokine production by immune system cells in patients with various forms of chronic sinusitis. Vestnik Otorinolaringologov.* 2021;(2):8–10.
5.	Alimov A.V., Shamansurova E.A., Mazinova D.E. *The role of* Chlamydophila pneumoniae *in the development of respiratory pathology in school-age children.Zhurnal Pediatriya (Tashkent).* 2015;(4):119–120.
6.	Arefyeva N.A., Aznabaeva L.F., Dayanov A.N., Trofimova N.P. *Intravenous immunoglobulins in the treatment of patients with chronic upper respiratory tract pathology.* In: *Proceedings of the 4th Scientific and Practical Conference "Topical Issues in Otorhinolaryngology."* Moscow; October 5–6, 2021. p. 109–110.
7.	Arifov S.S. *Clinical features, pathogenesis, and treatment of purulent otitis media and sinusitis depending on the degree of intoxication and*

	individual characteristics of the body. [Abstract of Dissertation for the Degree of Doctor of Medical Sciences]. Tashkent; 1999. 28 p.
8.	Arefyeva N.A., Aznabaeva L.F. *Immunocytological studies in otorhinolaryngology.* Russian Otorhinolaryngology. 2020;(2):222–225.
9.	Balyasinskaya G.L., Korovina N.A., Tatochenko V.K. *Antibacterial therapy of acute respiratory diseases in children: A guide for physicians.* Moscow; 2022.
10.	Bakhriddinova F.A., Bekturdiev Sh.S. *Complicated forms of chlamydial conjunctivitis.* In: *Proceedings of the 3rd International Scientific and Practical Conference "Proliferative Syndrome in Ophthalmology."* Moscow; November 29–30, 2024. Vol. 2. p. 87–88.
11.	. Bakhriddinova F.A., Bekturdiev Sh.S., Mirrakhimova S.Sh. *Use of the domestic non-steroidal anti-inflammatory eye ointment Fensulkal in the complex treatment of patients with paratrachoma.* Medical Journal of Uzbekistan. 2015;(3):70–72.
12.	. Bakhriddinova F.A., Karimova M.Kh., Eshboev E.Kh., Bekturdiev Sh.S. *Ocular forms of chlamydial infection.* Medical Journal of Uzbekistan. 2014;(4):138–141.
13.	. Bezrukova E.V., Belozerova L.A., Pashchinin A.N. *A method for assessing the effectiveness of treatment in patients with chronic rhinosinusitis.* Russian Otorhinolaryngology. 2019;(2):230–236.
14.	. Bekturdiev Sh.S. *Improvement of treatment methods for chlamydial eye lesions and clinical-laboratory evaluation of their effectiveness.* [Abstract of Dissertation for the Degree of Candidate of Medical Sciences]. Tashkent; 2017. 15 p.
15.	. Bekturdiev Sh.S., Abdurakhmonova U.M., Mirrakhimova S.Sh. *On the diagnosis and treatment of chlamydial eye lesions in patients with urogenital chlamydiosis.* In: *Proceedings of the Scientific and Practical Conference "Days of Youth Science."* Tashkent; April 22–23, 2014. p. 88.

16.	. Bekturdiev Sh.S., Makarova E.K. *Comparative evaluation of the effectiveness of medical treatment for chlamydial conjunctivitis.* In: *Proceedings of the Scientific and Practical Conference "Days of Youth Science."* Tashkent; April 21–22, 2015. p. 94–95.
17.	. Bekturdiev Sh.S., Egamberdieva S.M., Makarova E.K. *On the diagnosis and treatment of chlamydial conjunctivitis in newborns.* In: *Proceedings of the Scientific and Practical Conference with International Participation "Perspectives for the Development of Pediatric Ophthalmology."* Tashkent; May 4–5, 2015. p. 108–111.
18.	. Bekuzarova O.T., Kalagova S.K., Kalaev N.T. *The role of* Chlamydophila pneumoniae *in human ENT pathology.* Russian Otorhinolaryngology. 2020;(1):3–8.
19.	. Bogomilsky M.R., Strachunsky L.S. *Topical issues of pediatric otorhinolaryngology and pharmacotherapy of ENT diseases.* In: *Topical Issues of Pediatric Otorhinolaryngology in Pharmacotherapy of ENT Diseases.* Moscow; 2021. p. 21–30.
20.	. Bokovoy A.G., Grishina M.E., Novikova M.Yu., Lykova E.A. *Modern approaches to antibiotic use in bacterial complications of acute respiratory viral infections in children.* Kremlin Medicine. 1998;(4):34–37.
21.	. Bondarenko V.M., Rubakova E.I., Lavrova V.A. *Immunostimulating action of bacteria used as the basis for probiotic preparations.* Journal of Microbiology, Epidemiology and Immunobiology. 2019;(5):107–112.
22.	. Bondaruk V.V., Ponidelko S.N., Kiselev A.S., et al. *The etiopathogenetic role of chlamydiae in the course of chronic recurrent sinusitis.* Russian Rhinology. 2021;(2):171–172.
23.	. Bocharov A.F. *Clinical features and treatment of chlamydial laryngitis with Amiksin.* Vestnik Otorinolaringologii. 2020;(5):58–60.

24.	. Bratina E.E., Orlova O.E., Dmitriev G.A. *Some features of the life cycle of chlamydiae: atypical forms of existence (literature review).* Diseases Transmitted Sexually. 2016;(1):3–9.
25.	. Byrkhina V.V., Shelenkova V.V., Pasov V.V., Kozlov V.S. *Two-dimensional ultrasonography in the diagnosis of chronic sinusitis.* In: *Proceedings of the XVII Congress of Otorhinolaryngologists of Russia.* Nizhny Novgorod; June 7–9, 2016. p. 254.
26.	. Belova E.V. *Clinical and epidemiological aspects of chlamydial infection of the upper respiratory tract in children.* [Abstract of Dissertation for the Degree of Candidate of Medical Sciences]. Krasnoyarsk; 2018. 24 p.
27.	. Volkov A.G., Trofimenko S.L., Vinnikova N.V. *On the rational choice of drug therapy for chronic polypoid rhinosinusitis.* Russian Otorhinolaryngology. 2020;(2):272–276.
28.	. Ponidelko S.N., Poznyak A.L. *ENT lesions in patients with urogenital chlamydial infections with systemic manifestations: diagnostics, clinical course, and treatment prospects.* News of Otorhinolaryngology and Logopathology. 2021;(1):35–39.
29.	. Kapustina T.A., Kin T.I., Parilova O.V., Markina A.N., Belova E.V. *Diagnosis of chlamydial infection of the upper respiratory tract: a guide for physicians.* Krasnoyarsk; 2015. 19 p.
30.	. Kapustina T.A., Kin T.I., Parilova O.V., Markina A.N., Belova E.V. *Microbiology of chlamydiae and pathogenesis of chlamydial infection of the upper respiratory tract: a guide for physicians.* Krasnoyarsk; 2015. 24 p.
31.	. Belova E.V., Manchuk V.T., Kapustina T.A., Kin T.I. *Frequency of chlamydial infection of the upper respiratory tract in children.* Pacific Medical Journal. 2015;(3):64–65.

32.	. Belova E.V., Kapustina T.A., Markina A.N., Parilova O.V. *Prevalence of respiratory chlamydiosis in children.* In: *Topical Issues of Public Health Protection in the Regions of Eastern Siberia: Proceedings of the Siberian Branch of the Russian Academy of Medical Sciences.* Krasnoyarsk; 2016. p. 20–22.
33.	. Ponidelko S.N., Poznyak A.L., Glaznikov L.A., Nuralova I.V., Khlopunova O.V. *Generalized forms of chlamydial infection with predominant ENT involvement: diagnostics, clinical features, and treatment prospects.* In: *Proceedings of the 5th All-Russian Scientific and Practical Conference.* Saint Petersburg; 2021. p. 120–121.
34.	. Volkov A.G. *Chronic sinusitis.* In: *Otorhinolaryngology: National Guide.* Moscow; 2018. p. 475–496.
35.	. Vorobyev A.A. *Principles of classification and strategy for the use of immunomodulators in medicine.* Zhurnal Mikrobiologii, Epidemiologii i Immunologii. 2022;(4):93.
36.	. Galkina O.V., Katinas E.B., Lavrenova G.V., et al. *Local cytokine therapy in purulent sinusitis.* Medical Immunology. 2021;3(2):31.
37.	. Garyuk G.I., Garyuk O.G. *Effectiveness of the herbal multicomponent preparation Sinupret in the complex monotherapy of patients with acute and chronic rhinosinusitis.* Journal of Ear, Nose and Throat Diseases. 2014;(4):63–66.
38.	. Glazkova L.K., Akilov O.E. *Practical aspects of persistence of chlamydial infection.* Infections Transmitted Sexually. 2018;(4):29–34.
39.	. Glaine Abed El Naser, Proskurin A.I., Vishnevetskaya I.F. *Effect of Immunofan on the metabolic activity of immunocompetent cells in patients with chronic sinusitis.* In: *Proceedings of the Russian Scientific and Practical Conference.* Moscow; 2022. p. 321.
40.	. Goldin R.B., Lokhova M.D. *The immunofluorescence method in the diagnosis of viral infections, ornithosis, psittacosis, and trachoma.* In: *The Immunofluorescence Method in the Diagnosis of Infectious Diseases.*

	Moscow; 1999. p. 71–88.
41.	. Gomberg M.A., Soloviev A.M., Chernousov A.D. *Rationale for immunotherapy in the treatment of recurrent urogenital chlamydiosis.* Infections Transmitted Sexually. 2020;(2):30–35.
42.	. Gorbunov S.G., Gorelov A.V., Tatochenko V.K., Kharlamova F.S. *Etiology of acute respiratory diseases.* In: *Acute Respiratory Diseases in Children: Treatment and Prevention.* Moscow; 2024. p. 10–15.
43.	. Granitov V.M. *Chlamydioses.* Moscow: Medkniga; Nizhny Novgorod: NGMA Publishing House; 2020. 197 p.
44.	. Demchenko E.V., Ivanchenko G.F., Prozorovskaya K.N., et al. *Clinical features and treatment of chlamydial laryngitis with Amiksin.* Vestnik Otorinolaringologii. 2020;(5):58–60.
45.	. Dmitriev G.A., Kiseleva V.N., Orlova O.E. *Laboratory diagnosis of urogenital chlamydiosis: A guide for physicians.* Moscow: Ministry of Health of the Russian Federation, Central Research Institute of Skin and Venereal Diseases; 1999. 19 p.
46.	. Evsyukova I.I. *Chlamydial infection in newborns.* Pediatrics. 2017;(3):77–80.
47.	. Evsyukova I.I. *Chlamydial infection: diagnosis, prevention, and treatment.* Saint Petersburg; 1995. 16 p.
48.	. Zhevachevsky N.G. *Comparative analysis of methods for diagnosing chlamydiosis.* Clinical Laboratory Diagnostics. 2021;(2):36–38.
49.	. Zaitseva O.V. *Chlamydial infection: a new perspective on the problem.* Therapeutic Archive. 2021;73(11):35–39.
50.	. Ziborova N.V., Makkaev Kh.M., Shevrygin B.V. *Microbial flora of the maxillary sinuses in various forms of sinusitis.* In: *Proceedings of the 16th Congress of Otorhinolaryngologists of the Russian Federation.* 2021. p. 585–589.

51.	. Ilyin I.I. *Issues of epidemiology of human chlamydial infections.* Vestnik Dermatologii. 2013;(4):37–39.
52.	. Ismagilov Sh.M., Mukhammadiev R.A., Ivanov A.V. *Clinical and microbiological characteristics of patients with chronic rhinosinusitis under different anthropotechnogenic loads.* Russian Otorhinolaryngology. 2019;(2):305–307.
53.	. Kalashnikova S.Yu., Sergeev S.V. *Epidemiological, clinical, and pathogenetic features of polypoid rhinosinusitis in different age groups.* Russian Otorhinolaryngology. 2019;(2):308–311.
54.	. Ketlinskiy S.A., Ishchenko A.M. *Cytokines and their antagonists: theory and practice.* Medical Immunology. 2016;1(3–4):16.
55.	. Kozlov I.V., Pyshnyy D.V. *Functional evaluation of the effectiveness of surgical treatment of chronic rhinosinusitis in flight personnel.* Russian Otorhinolaryngology. 2020;(2):314–318.
56.	. Kozlova V.I., Pukhner A.F. *Viral, chlamydial and mycoplasmal diseases of the genitals: A guide for physicians.* Saint Petersburg; 2000. 572 p.
57.	. Kolkova N.N., Martynova V.R. *On the diagnosis of chlamydial infections.* Clinical Laboratory Diagnostics. 1999;(2):20–21.
58.	. Kondrashev P.A., Podnos A.L., Batyzheva A.A. *Some features of microflora in chronic maxillary sinusitis and its effect on mucociliary activity of the nasal mucosa epithelium.* Russian Otorhinolaryngology. 2020;(2):323–328.
59.	. Korkmazov M.Yu., Kornova N.V., Chinkov N.A., Nokhrin D.V., Shisheva A.K. *Assessment of local and systemic immunity in patients with polypoid rhinosinusitis during complex treatment with physical therapy methods.* Russian Otorhinolaryngology. 2020;(2):332–337.
60.	. Kryukov A.I., Bondareva G.P., Terekhova A.O. *The role of mycoplasmal and chlamydial infections in the course of the asymptomatic triad.* Russian Otorhinolaryngology. 2020;(2):337–339.

61.	. Kurbanov F.F., Svistushkin V.M., Gerasimenko M.Yu., Filatova E.V., Mustafayev D.M., Kurbanova E.A. *Fluctuorization in the complex treatment of patients with acute maxillary sinusitis.* Russian Otorhinolaryngology. 2020;(2):341–345.
62.	. Kuyan Yu.S., Sergeev A.V., Protasov P.G., Khamidova D.M., Mokronosova M.A. *Eosinophilic cationic protein as a marker of nasal mucosal inflammation.* Russian Otorhinolaryngology. 2019;(2):346–351.
63.	. Linkov V.I., Tsurikova G.P., Nuralova I.V., et al. *The significance of chlamydial infection in the development of chronic inflammatory diseases of the pharynx.* News of Otorhinolaryngology and Logopathology. 1999;3(4):146.
64.	. Lobzin Yu.V., Poznyak A.L., Simbirtsev A.S., et al. *Comparative efficacy of Bestim, Immunofan, Cycloferon, and Glutoxim in the complex therapy of chlamydial infections with systemic manifestations in young adults.* In: *Proceedings of the 6th Russian-Italian Scientific Conference.* Saint Petersburg; 2021. p. 142–143.
65.	. Lobzin Yu.L., Poznyak A.L., Raevsky K.K., et al. *Diagnosis and treatment of generalized forms of chlamydial infections in young people.* Saint Petersburg; 2000. 91 p.
66.	. Lopatin A.S., Tryakina E.G. *Long-term low-dose macrolide therapy for chronic rhinosinusitis.* Russian Rhinology. 2017;(4):38–41.
67.	. Marchenko A.A., Morchenko V.M., Marchenko L.A., Rakitina E.L. *Status of natural resistance factors in certain pathological conditions.* Russian Otorhinolaryngology. 2019;(2):361–364.
68.	. Makhmudov M.U., Dzhabbarov K.D. *Immunological features of chronic sinusitis associated with chlamydial infection.* Russian Otorhinolaryngology. 2019;(2):364–368.
69.	. *Medical Laboratory Diagnostics (Programs and Algorithms): Handbook.* Ed. by Prof. A.I. Karpishchenko. Saint Petersburg: Intermedica; 2018. 304 p.

70.	. Mirazizov K.D., Dzhabbarov A.K. *Clinical features and treatment of purulent ethmoiditis in anaerobic non-clostridial infection.* Vestnik Otorinolaringologii. 1998;(5):43–45.
71.	. Morton R.S., Kinghorn J.R. *Urogenital chlamydial infection: reassessment of data and hypotheses.* Infections Transmitted Sexually. 2000;(2):4–15.
72.	. Mukhitdinov U.B., Noraliev R.B. *Frequency of sinusitis in children.* In: *Proceedings of the Russian Scientific and Practical Conference "Modern Problems of Diseases of the Upper Respiratory Tract and Ear."* Moscow; 2022.
73.	. Nikolaev M.P., Trofimov E.I., Daykhes I.A., Fuki E.M., Reshulsky S.S. *Atypically occurring chronic rhinosinusitis.* Russian Otorhinolaryngology. 2010;(2):381–385.
74.	. Oriel J.D., Ridgway J.L. *Chlamydiosis.* Ed. by V.V. Delektorsky. Moscow: Meditsina; 1984. 192 p.
75.	. *Otorhinolaryngology.* Ed. by I.B. Soldatov, V.R. Gofman. Saint Petersburg; 2000. 472 p.
76.	. Paltsev M.A. *Cytokines and their role in intercellular interactions.* Archives of Pathology. 1999;58(6):3–6.
77.	. Pigarevsky V.E. *Hypothesis on resorptive cellular resistance as a specific form of the body's antimicrobial defense.* Archives of Pathology. 2012;(8):40–45.
78.	. Piskunov G.Z., Kosyakov S.Ya., Angotoeva I.B., Atanesyan A.G. *Modern standards for the diagnosis and treatment of various forms of rhinosinusitis.* Otorhinolaryngology. 2014.
79.	. Piskunov S.Z., Piskunov G.Z. *Diagnosis and treatment of inflammatory processes of the nasal and paranasal mucosa.* Voronezh: Voronezh State University Press; 1999. 181 p.
80.	. Volkov A.G., Trofimenko S.L. *Clinical manifestations of secondary immunodeficiency in ENT diseases.* Rostov-on-Don; 2018. 203 p.

81.	. Likhanova M.A., Mingalov N.V., Lebedova R.N. *Influence of intracellular pathogens on recurrence of polypoid rhinosinusitis.* Russian Otorhinolaryngology (Supplement). 2017:313–317.
82.	. Lopatin A.S., Tryakina E.G. *Long-term low-dose macrolide therapy for chronic rhinosinusitis.* Russian Rhinology. 2017;(4):38–41.
83.	. Piskunov G.Z., Piskunov S.Z. *Clinical Rhinology.* Moscow; 2006. 560 p.
84.	. Tulebayev R.K., Dzhandayev S.Zh., Papulova N.M. *Acute and chronic sinusitis.* Astana; 2014. 74 p.
85.	. Kryukov A.I. *Diagnosis and treatment of chronic sinusitis: methodological recommendations.* Moscow; 2015. 22 p.
86.	. Piskunov S.Z., Piskunov G.Z., Velnov I.V., et al. *General and local conservative treatment of acute and chronic maxillary sinusitis.* Russian Rhinology. 1999;(1):5–15.
87.	. Pluzhnikov M.S., Lavrenova G.V., Galkina O.V., et al. *Local use of Roncoleukin in acute purulent sinusitis.* Medical Immunology. 1999;1(3–4):128.
88.	. Plyutto A.M. *Detection of chlamydial infection by indirect cytological signs.* Clinical Laboratory Diagnostics. 1998;(8):19–21.
89.	. Poznyak A.L., Lobzin Yu.V. *Etiotropic therapy of generalized forms of chlamydial infection: modern drugs and rational treatment regimens.* In: *Topical Issues of Antibacterial Therapy of Inflammatory Diseases of the Urogenital Tract: Conference Proceedings.* Saint Petersburg; 2010. p. 13–17.
90.	. Poznyak A.L., Lobzin Yu.V., Simbirtsev A.S., et al. *Principles and schemes of rational cytokine immunotherapy for chlamydial infection with systemic manifestations.* Russian Journal of HIV/AIDS and Related Problems. 2021;5(1):57–58.

91.	. Poznyak A.L., Lobzin Yu.V., Simbirtsev A.S., et al. *Principles of rational immunotherapy for generalized forms of chlamydial infection in young adults.* Terra Medica. 2020;(2):5–10.
92.	. Poznyak A.L., Lobzin Yu.V., Timchenko V.N., et al. *Rational therapy regimens for chlamydial infection in children.* Bolnitsa (The Hospital). 2020;(11–12):10.
93.	. Poznyak A.L., Ponidelko S.N. *ENT organ involvement in patients with urogenital chlamydial infections with systemic manifestations: diagnostics, clinical picture, and treatment prospects.* News of Otorhinolaryngology and Logopathology. 2021;(3):35–39.
94.	. Volkov A.G. *Otorhinolaryngology: National Guide.* Moscow: Meditsina; 2018. p. 475–491.
95.	. Raytselis I.V. *Clinical significance of biological properties of microorganisms for predicting the course and treatment of patients with purulent maxillary sinusitis.* [Abstract of dissertation for the degree of Candidate of Medical Sciences]. Orenburg; 2010. 27 p.
96.	. Piskunov G.Z., Piskunov S.Z., Kozlov V.S., Lopatin A.S. *Diseases of the nose and paranasal sinuses.* In: *Endomicro Surgery.* Moscow; 2013. 188 p.
97.	. Lopatin A.S. *Acute rhinosinusitis: is antibiotic therapy always necessary?* Medical Department. 2012;(4).
98.	. Teplova S.N., Alekseev D.A. *Secretory immunity.* Ural Branch of the Russian Academy of Sciences, Chelyabinsk; 2012. 200 p.
99.	. Savenkova M.S. *Chlamydial and mycoplasmal infection in pediatric practice.* Consilium Medicum. 2015;7(1):3–10.
100.	. Poznyak A.L., Simbirtsev A.S., Smirnov M.N., et al. *Combined use of Betaleukin and Roncoleukin in immunotherapy of generalized forms of chlamydial infection.* Russian Journal of HIV/AIDS and Related Problems. 2010;4(1):92.
101.	. Polyak M.S. *Atherosclerosis, chlamydiae, and prospects of antibiotic*

	therapy. Lectures on Pharmacotherapy. 1999;(9):14 p.
102.	. Roskin G.I., Levinson L.B. *Microscopic Technique.* Moscow: State Publishing House “Soviet Science”; 1997. 467 p.
103.	. Ryazantsev S.V., Naumenko N.N., Zakharova G.P. *Principles of etiopathogenetic therapy of acute sinusitis: methodological guidelines.* Saint Petersburg; 2016. 44 p.
104.	. Sadykova G.Z. *Indicators of cellular and humoral immunity in children with acute inflammation of the maxillary sinus.* Pediatrics and Pediatric Surgery of Kazakhstan. 2016;1:18–20.
105.	. Semenov D.M. *Clinical forms of chlamydial infection.* Medical News. 2021;(4):25–30.
106.	. Serebryansky Yu.E., Afanasyev S.S., Denisov L.A., et al. *Cytokines in immunorehabilitation of infectious patients.* Russian Medical Journal. 1999;(3):41–50.
107.	. Sidorenko S.V. *Antibacterial therapy of infections caused by C. trachomatis.* Antibiotics and Chemotherapy. 2021;46(2):1–8.
108.	. Sedykh T.K., Chernyshenko I.O., Rusetsky Yu.Yu. *Interpretation of microbiological examination results of adenoids depending on the method of biomaterial sampling.* In: *IV Scientific and Practical Conference “Topical Issues in Otorhinolaryngology”*. Moscow; Oct 5–6, 2021. p. 138–139.
109.	. Simbirtsev A.S. *Interleukin-2 and its receptor complex in immune regulation.* Immunology. 1999;(6):3–8.
110.	. Strachunsky L.S., Kamanin E.I., Tarasov A.A., et al. *Antibacterial therapy of sinusitis: methodological guidelines for clinicians.* 2012.
111.	. Sumarokov A.B., Lyakishev A.A. *Chlamydial infection caused by Ch. pneumoniae and atherosclerosis.* Clinical Medicine. 1999;(7):5–10.
112.	. Sakovich A.R., Semak L.I. *Assessment of general reactivity in patients*

	with acute purulent sinusitis using hematologic indices. Russian Otorhinolaryngology. 2009;(2):269–273.
113.	. Babiyak V.I., Nakatis Ya.A. *Clinical Otorhinolaryngology: A Guide for Physicians.* Hippocrates; 2005. p. 390–407.
114.	. Palchun V.T., ed. *Otorhinolaryngology: National Guide.* Moscow: GEOTAR-Media; 2008. 960 p.
115.	. Sukhinin V.P. *Condition of the nasal and maxillary sinus mucosa in patients with chronic sinusitis of chlamydial etiology according to light and electron microscopy.* News of Otorhinolaryngology and Logopathology. 2021;(4):82–86.
116.	. Tarasov L.N., Grigoryev E.G. *Syndrome of maternal and neonatal chlamydial infection.* Ophthalmology Journal. 1994;(4):233–236.
117.	. Bykova V.P., Kalinin D.V. *Mucosal immune barrier in modern interpretation.* Russian Rhinology. 2019;(1):40–43.
118.	. Nazarochkin Yu.V., et al. *Determination of serum cytokine levels in patients with rhinosinusitis and diabetes mellitus for early diagnosis of systemic inflammatory response syndrome.* Russian Otorhinolaryngology. 2019;(2):241–245.
119.	. Timchenko V.N., Poznyak A.L., Yakovlev A.O., et al. *Use of the modern macrolide antibiotic "Vilprafen" in the treatment of chlamydial infection in children.* In: *Abstracts of the Scientific-Practical Conference "Infectious Diseases: Diagnosis, Treatment, Prevention."* Saint Petersburg; 2020. p. 254.
120.	. Evsyukova E.V., Fedoseev G.B., Savicheva A.M. *Chlamydial infection and aspirin-induced bronchial asthma.* Pulmonology. 2002;(5):64–86.
121.	. Gurov A.V. *Edema of the upper respiratory mucosa: how to manage it?* Russian Medical Journal. 2009;(19):1254–1260.
122.	. Piskunov G.Z. *Causes of increasing prevalence of nasal and paranasal sinus diseases.* Russian Rhinology. 2009;(2):7–9.

123.	. Arefyeva N.A., Guseva U.D., Kudakaeva R.Kh. *Microbial composition of the upper airway mucosa in hospitalized patients with rhinosinusitis.* Russian Rhinology. 2009;(2):9–10.
124.	. Palchun V.T., Kunelskaya N.L., Artemyev M.E. *Microbial landscape of acute purulent sinusitis.* In: *Advances in Medical Mycology: Proceedings of the First All-Russian Congress on Medical Mycology.* Moscow; 2023;2:252–254.
125.	. Tolchenitsyn I.A., Vavin V.V., Mingaliev N.V. *Features of treatment of chronic odontogenic maxillary sinusitis.* Russian Otorhinolaryngology. 2019;(2):439–442.
126.	. Filin V.A., Rudintseva N.V., Sitkina L.N. *Infection caused by Chlamydia trachomatis in children: frequency, diagnosis and treatment.* Pediatrics. 1999;(1):20–22.
127.	. *Chlamydioses: Clinic, Diagnosis, and Treatment. Methodological Guidelines.* Moscow; 1996. 22 p.
128.	. Khlopunova O.V., Poznyak A.L., Dobrynin V.M., et al. *Bacteroides infection in young adults: diagnosis and clinical features.* In: *Topical Issues of Antibacterial Therapy of Inflammatory Diseases of the Urogenital Tract: Conference Proceedings.* Saint Petersburg; 2000. p. 26–27.
129.	. Chuev P.N., Pukhlyk S.M., Fadeeva Z.V. *Cultivation and identification of anaerobic pathogens of purulent-septic ENT diseases under modern conditions.* Journal of Ear, Nose and Throat Diseases. 2001;(2):3–37.
130.	. Dzhenzhera G.E., Ovchinnikov A.Yu., Ovcharenko S.I. *Systemic antibacterial therapy in complex treatment of patients with exacerbation of bacterial rhinosinusitis.* Vestnik Otorhinolaryngologii. 2019;(3):356–358.
131.	. Molochkov V.A., Molochkov A.V., Aksenova O.A. *Chlamydial and mycoplasmal infections in inflammatory pathology of the urogenital tract: A manual for physicians.* Moscow; 2017. 22 p.

132.	. Shamsiev D.F. *Cytological examination of nasal smears in patients with chronic rhinosinusitis.* In: *Proceedings of the Conference "Topical Issues in Otorhinolaryngology."* Moscow; 2008. p. 104.
133.	. Shamsiev D.F. *Improvement of diagnosis and treatment of chronic inflammatory diseases of the paranasal sinuses.* [Abstract of Doctor of Medical Sciences dissertation]. Tashkent Medical Academy; 2019. 42 p.
134.	. Romanova M.A. *Rovamycin in the complex therapy of recurrent bronchitis caused by C. pneumoniae and M. pneumoniae in children.* In: *Proceedings of the 5th Russian Congress of Pediatric Infectiologists.* Moscow; 2006. p. 137.
135.	. Romanova M.A. *Role of carnitine chloride in the complex therapy of recurrent bronchitis associated with C. pneumoniae and M. pneumoniae infection.* In: *Proceedings of the 7th Russian Congress of Pediatric Infectiologists.* Moscow; 2018. p. 124–125.
136.	. *Medico-social and clinical characteristics of patients with inflammatory pathology of the nose and paranasal sinuses associated with chlamydial infection.* [Abstract of Candidate of Medical Sciences dissertation]. Krasnoyarsk; 2019. 25 p.
137.	. Shamsiev D.F. *Clinical physiology of the nose and paranasal sinuses: Methodological guidelines.* Tashkent; 2008. 16 p.
138.	. Shamsiev D.F. *Cytological examination of nasal smears in patients with chronic rhinosinusitis.* In: *Proceedings of the Conference "Topical Issues in Otorhinolaryngology."* Moscow; 2018. p. 104.
139.	. Shanturov A.G., Nosulya E.V. *Some issues of clinical classification of sinusitis.* Russian Rhinology. 1998;(2):21.
140.	. Shubin S.V., Orlova O.E., Zotova I.F., et al. *On the persistence of chlamydiae in Reiter's disease.* In: *Actual Microbiological and Clinical Problems of Chlamydial Infections.* Moscow; 1990. p. 61–62.

141.	. Shchubin M.N. *Features of diagnosis and treatment of deep latent sinusitis.* In: *Proceedings of the XVII Congress of Otorhinolaryngologists of Russia.* Nizhny Novgorod; 2016. p. 255–256.
142.	. Eidelstein I.A. *Fundamental changes in the classification of chlamydiae and related microorganisms of the order Chlamydiales.* Clinical Microbiology and Antimicrobial Chemotherapy. 1999;1(1):5–12.
143.	. Yakovlev V.M., Novikov A.I. *Vascular endothelium and chlamydial infection.* Moscow: Meditsina; 2020. 172 p.
144.	. Yampolsky S.Z. *Drop irrigation of the paranasal sinuses as a method of pathogenetic therapy for rhinogenic sinusitis.* In: *Proceedings of the Russian Scientific and Practical Conference "Modern Problems of Diseases of the Upper Respiratory Tract and Ear."* Moscow; 2022.
145.	. Yanov Yu.K., Konoplev O.I., Naumenko N.N., Antusheva I.A. *Antibiotics with a high safety profile for intestinal microflora: new perspectives for antibiotic therapy of acute bacterial rhinosinusitis.* Russian Otorhinolaryngology. 2010;(2):465–474.
146.	. Yanov Yu.K., et al. *Practical recommendations for antibacterial therapy of sinusitis.* Clinical Microbiology and Antimicrobial Chemotherapy. 2003;5(2):167–174.
147.	Adouble-blind, randomized, placebo-controlledtrialofmacrolideinthetreatmentofchronicrhinosinusitis / WallworkB.[et al.] // Laryngoscope. -2006. –Vol.116. –P. 143-148.
148.	W. Huvenne [et al]. Chronic rhinosinusitis with and without nasal polyps: what is the difference? // Curr Allergy Asthma Rep. -2009. –Vol.9, №3. –P.213-220.
149.	Marple B.F., [et al]. Diagnosis and management of chronic rhinosinusitis in adults. // Postgrad Med. -2009. –Vol.121, №6. P.121-139.
150.	Ferguson B.J., Otto B.A., Pant H. When surgery, antibiotics, and steroids fail to resolve chronic rhinosinusitis. // Immunol Allergy Clin North Am. -2009. –Vol.29, №4. –P.719-732.

151.	Hellings P.W., Hens G. Rhinosinusitis and the lower airwais // Immunol Allergy Clin North Am. -2019. –Vol .29, №4. –P733-740.
152.	Zhu L., [et all]. Revison endoscopic sinus surgery and combined therapy for recurrent sinusitis. // Lin Chung Er Bi Yan Hou Tou Jing Wai Ke Za Zhi. -2019. –Vol.23, №11. –P.488-490.
153.	Wallwork B., [et al]. Clarithromycin and prednisolone inhibit cytokine production in chronic rhinosinusitis. // Laryngoscope. -2002. –Vol.112, №10. –P.1827-1830.
154.	Suzuki H. Mode of action of long-term macrolide therapy for chronic sinusitis in the light of neutrophil recruitment / Suzuki H., R. Ireda // Curr. Drug Targets Inflamm. Allergy. -2002. –Vol .1. –P.117-126.
155.	Araujo E., Palombini B.C., Cantarelli V. et al. Microbiology of middle meatus in chronic rhinosinusitis Am ORhinol 2003; Jan-feb;17(1): p. 9-15.
156.	Taxy J.B. Paranasal Fungal Sinusitis: Contribution of Histopatology to Diagnosis. A report of 60 Cases and Literature Review. // Am JSurg Pathol. - 2006; 30:713-720.
157.	Blasi F., Boman J., Esposito G. et al. Chlamydia pneumoniae DNA detection in peripheral blood mononuclear cells is predictive of vascular infection. // J. Infect. Dis. - 1999. - Vol.180 - №6 - P.2074-2076.
158.	Brook I, Shah K Sinusitis in neurologically impaired children. // Otolaryngol Head Neck Surg -1998 - Vol. 119 - P.357-360.
159.	Brook I, Yocum P, Frazier E.H. Bacteriology and beta-lactamase activity in acute and chronic maxillary sinusitis. // Arch Otolaryngol Head Neck Surg., 2019 -Vol.l22(4)-P.418-422.
160.	Campbell L.A., O'Brien E.R., Cappuccio A.L. et al. Detection of Chlamydia pneumoniae TWAR in Human Coronary Atherectomy Tissues. // J. Infect. Dis. -1995.-Vol.172.-P.585-588.
161.	Cervin A., Wallwork B. Anti-inflammatory effects of macrolide antibiotics in the treatment of chronic rhinosinusitis // Otolaryngol. Clin.Noth Am. -2015. -№38(6). –C.1339-1350.

162.	Dominque G.Y., Hellistron W.J.G. Prostatitis. Department of Urology and Department of Microbiology and Immunology, Tulane University School of Medicine, New Orlean, Lousiana 70112, USA // Clin. Microbiology Rev.-1998. -Vol.11.-P.604-613.
163.	Gaillat J. Clinical manifestations of Chlamydia pneumoniae infections. // Rev. Med. Interne. -1996. -Vol.17. №12. -P.987-991.
164.	Gaydos C.A. Growth in vascular cells and cytokine production by Chlamydia pneumoniae. // J Infect Dis. -2000. -Vol.181 -P.473-478.
165.	Gaydos C.A., Summersgill J.T., Sahney N.N. et al. Growth characteristics of Chlamydia pneumoniae in macrophages and endothelial cells. // In: Orfila J., Byrne G.L., Cherneskey M.A., et al., eds. Chlamydial infections. Bologna, Italy: Societa Edittrice Esculapio. -1994. -P.216-219.
166.	Gnarpe H., Gnarpe J., Gastrin B. et al. Chlamydia pneumoniae and myocarditis .// Scand. J. infect. Dis. -1997. -Vol.104. -P.50-52.
167.	Grayston J.T. Infections Caused by Chlamidia pneumoniae Strain TWAR. // Clinical Infect. Dis. -1992. -Vol.15. -P.757-761.
168.	Grayston J.T., Campbell L.A., Kuo C.C. et al. A new respiratori tract pathogen: Chlamydia pneumoniae strain TWAR. Hi. Infect. Dis. -1990. -Vol.161.-P.618-625.
169.	Grayston J.T., Kuo C.C., Campbell L.A. et al. Chlamidia pneumoniae Strain TWAR and atherosclerosis. // Eur. Heart J. -1993.-Vol.14.-P.66-71.
170.	Gurr P.A., Chakraverty A., Callanan V. The detection of Mycoplasma pneumoniae in nasal polyps. // Clin Otolaryngol -1996. -Vol.21 - P.269-273.
171.	Bhattacharyya, N. Clinical and symptom criteria for the accurate diagnosis of chronic rhinosinusitis [text] / N. Bhattacharyya // Laryngoscope. -2006. –Vol. 116 (7 Pt. 2. –Suppl. 110). –P. 1-22.
172.	Hashiguchi K., Ogawa H., Suzuci T. et al. Isolation of Chlamidia pneumoniae from the Maxillary Sinus of a Patient with Purulent Sinusitis. // Clinical. Infect. Dis. -1992. -Vol.15. -P.570-571.

173.	Higuchi M.L., Sambiase N., Palomino S. et al. Detection of mycoplasma pneumoniae and chlamydia pneumoniae in ruptured atherosclerotic plaques. // Braz J Med Biol Res. -2000 -Vol.33, №9. -P.1023-1026.
174.	Hodinca R.L., Davis CD., Choong J. et al. Ultrastructural study of endocytosis of Chlamydia trachomatis by McCoy cells // Infect. Immun. - 1988. -Vol.56. -P.1456-1463.
175.	Hodinca R.L., Wyrick P.B. Ultrastructural study of mode of entry of Chlamydia psittaci into L-929 cells // Infect. Immun. -1986. -Vol.54. -P.855-863.
176.	Karvonen V., Tuomilehto J., Pitkaniemi J. et al. The epidemic cycle ofChlamydia pneumoniae infection in eastern Finland, 1972-1987. // EpidemiolInfect 1993.-Vol.110.-P.349-360.
177.	Kaupinen M.T., Herva E., Kujla P. et al. The Etiology of Community-Acquired Pneumonia among Hospitalized Patients during a Chlamydia pneumoniae Epidemic in Finland. // J Infect Dis. -1995. -Vol.172 -P.1330-1335.
178.	Kawauchi H. Cytokine-modulators (Suplatas tosilate/Macrolide): hov to down regulate the mucosae inflammation? // Россиийск.Ринология. -2016. -№2. –С. 42.
179.	Kawai A., Sato Y., Yamamoto H. et al. Studies on otolaryngeal Chlamydia trachomatis infection province. // Nippon Jibiinkoka Gakkai Kaiho. -2013. -Vol.96,111.-P.371-378.
180.	Kennedy C.A., Jyonouchi H., Kajander K.C. et al. Middle ear pathologic changes associated with chronic anaerobic sinusitis in rabbits. // Laryngoscope, 1999 -Vol.109(3)-P.498-503.
181.	Lobau S. Molecular cloning, sequence analysis, and functional characterrization of the lipopolysaecharide biosynthetic gene kdtA encoding 3-dcoxy-alpha-D-manno-octulosonic acid transferase jf Chlamydia pneumoniae strain TW-183 // Mol. Microbiol. -2023. -Vol.l8.-P.391-399.

182.	Lund V., Gwaltney J., Baguero F.et al. Infectious rhinosinusitis in adults: classification, etiology and management //J. Ear., Nose and Throat. -1997. -Vol.76, suppl. -P.22.
183.	Nasralla M., Haier J., Nicolson G.L. Multiple mycoplasmal infections detected in blood of patients with chronic fatigue syndrome and/or fibromyalgia syndrome // Eur. J. Clin. Microbiol. Infect. Dis. - 1999. -Vol.18. -№12 -P.859-865.
184.	Ogawa H, Hashiguchi K, Kazuyama Y. Recovery of Chlamydia pneumoniae and Chlamydia trachomatis in a patient with recurrent tonsillitis, bronchitis and otitis media with effusion.// Kansenshogaku Zasshi.-1991.-Vol. 65, №2. -P.234-238.
185.	Ogawa H., Fujisawa T., Kazuyama Y. Isolation of Chlamydia pneumoniae from Middle Ear Aspirates of Otitis Media with Effusion: A Case Report. // J. Infect. Dis. - 1990.-Vol. 162-P. 1000-1001.
186.	Ottolenghi A., Magliano E.M., De Chiara A. et al. Chlamydia andpharyngotonsillitis in childhood.// Minerva Pediatr.-2019.-Vol.41, №4. =. P.209-214.
187.	Pawankar R. Low dose long term macrolide therapy in chronic sinusitis with nasal polyps //Российск. Ринолог.-2006. -№2. –С.45.
188.	Savolainen S., Jousimies-Somer H., Kleemola M. et al. Serological evidence of viral or Mycoplasma pneumoniae infection in acute maxillary sinusitis. 7/ Eur J Clin Microbiol Infect Dis - 1989 -Vol.8 - P.131-135.
189.	Shamsiev D.F. Antibiotics in treatment of bacterial rhinosinusitis.// European Archives of Otorhinolaryngology and Head and Neck. -Vol.264, -Suppl. 1, -2017. p. 335, Abstract № RP 98
190.	Shamsiev D.F. Endoscopic surgery of the maxillary sinus.// Abstract book of the 10th International Congress of European Association for Endoscopic Surgery. 2-5 June2002.-Lisboa, Portugal. Abstract №0061. P.22

191.	Shamsiev D.F. Diagnostic maxillary sinus endoscopy. // Abstract book of 5th Europeaan Congress of Otorhinolaryngology. Rodos-Kos,Greece. -2004. -Abstract № 142. – P. 207.
192.	Schachter L. Chlamydial infections. // N. Engl. J. Med. -1978. -Vol. 298 - P. 428-435.
193.	Shehme-Avni L, Lieterman D. // Chlamydia pneumonial - born with ciliostasis in ciliated bronchial epithelial cells. // J Infect Dis. -1995. -Vol.171 -P. 1274-1278.
194.	Shor A, Phillips J.I. Chlamydia pneumoniae and atherosclerosis. // Journal of the American Medical Association. -1999. -Vol.282 -P.2071-2073.
195.	Stierna P, Kumlien J, Carlsoo B Experimental sinusitis in rabbits induced by aerobic and anaerobic bacteria: models for research in sinusitis. // J Otolaryngol., 1991 -Vol.20(6) -P.376-378.
196.	Stille W. Arteriosklerose - eine Infektion durch Chlamydia pneumoniae.// Dtsch. Med. Wschr. -1997. -Vol.122, №36. -P.1086-1091.
197.	Ward M.E. The immunobiology and immunopathology of Chlamydial infections. // Acta path, microbiol. immunol. Scand. -1995. -Vol.103. -P.769-796.
198.	Westrin K.M., Stierna P., Carlsoo B. et al. Mucosal fine structure in experimental sinusitis. // Ann Otol Rhinol Laryngol., 1993 -Vol. 102(8 Pt 1) - P.639-
199.	Wolf K., Fischer E., Hackstadt T. // Ultrastructural Analysis of Developmental Events in Chlamydia pneumoniae-Infected Cells // Infect. Immun. -2010. -Vol. 68. -P.2379-2385.
200.	Yamada S. Chlamydia pneumoniae infection in children with lower respiratory tract infections. // Kurume. Med. J. -2015.-Vol.42 -N2. - P. 107-120.

201.	Yamazaki T., Nakada H., Sakurai N. et al. Transmission of Chlamydia pneumoniae in Young Children in a Japanese Family. // J. Infect. Dis. -1990. -Vol.162.-P.1390-1392.
202.	Yang Z.P., Cummings P.K., Patton D.L. et al. Ultrastructural lung pathology of experimental Chlamydia pneumoniae pneumonitis. // J. Infect. Dis. -2024. -Vol.170-P. 464-467.
203.	Yang Z.P., Kuo C.C., Grayston J.T. Systemic dissemination of Chlamydia pneumoniae following intranasal inoculation in mice. // In: Orfila J., Byrne G.L., Cherneskey M.A., et al., eds. Chlamydial infections. Bologna, Italy: Societa Edittrice Esculapio. -2014. -P. 594-552.

LIST OF ABBREVIATIONS

ACE – angiotensin-converting enzyme

WHO – World Health Organization

ONH – optic nerve head

ELISA – enzyme-linked immunosorbent assay

CT – computed tomography

MRI – magnetic resonance imaging

OCT – optical coherence tomography

PNS – paranasal sinuses

PCR – polymerase chain reaction

CRP – C-reactive protein

CCST – cavernous sinus thrombosis

MFA – maxillofacial area

MFCS – maxillofacial surgeon

FESS – functional endoscopic sinonasal surgery